AGU100 ADVANCING EARTH AND SPACE SCIENCE

Water Resources Research

RESEARCH ARTICLE
10.1029/2019WR025875

# Multiresolution Approach to Condition Categorical Multiple-Point Realizations to Dynamic Data With Iterative Ensemble Smoothing

**D.-T. Lam[1], P. Renard[1], J. Straubhaar[1], and J. Kerrou[1]**

[1]Centre for Hydrogeology and Geothermics, University of Neuchâtel, Neuchâtel, Switzerland

**Key Points:**
- A novel multiresolution parameterization is used to condition categorical multiple-point direct sampling simulations to dynamic data
- Dynamic data are assimilated with an iterative ensemble smoother by updating continuous latent variables at the coarsest resolution
- A robust convergence towards consistent geological structures and a good data match is illustrated on a synthetic groundwater flow problem

**Correspondence to:**
D.-T. Lam,
dan-thuy.lam@unine.ch

**Citation:**
Lam, D.-T., Renard, P., Straubhaar, J., & Kerrou, J. (2020). Multiresolution approach to condition categorical multiple-point realizations to dynamic data with iterative ensemble smoothing. *Water Resources Research*, *56*, e2019WR025875. https://doi.org/10.1029/2019WR025875

Received 1 JUL 2019
Accepted 21 DEC 2019
Accepted article online 26 DEC 2019

**Abstract** A new methodology is presented for the conditioning of categorical multiple-point statistics (MPS) simulations to dynamic data with an iterative ensemble smoother (ES-MDA). The methodology relies on a novel multiresolution parameterization of the categorical MPS simulation. The ensemble of latent parameters is initially defined on the basis of the coarsest-resolution simulations of an ensemble of multiresolution MPS simulations. Because this ensemble is non-multi-Gaussian, additional steps prior to the computation of the first update are proposed. In particular, the parameters are updated at predefined locations at the coarsest scale and integrated as hard data to generate a new multiresolution MPS simulation. The performance of the methodology was assessed on a synthetic groundwater flow problem inspired from a real situation. The results illustrate that the method converges towards a set of final categorical realizations that are consistent with the initial categorical ensemble. The convergence is reliable in the sense that it is fully controlled by the integration of the ES-MDA update into the new conditional multiresolution MPS simulations. Thanks to a massively reduced number of parameters compared to the size of the categorical simulation, the identification of the geological structures during the data assimilation is particularly efficient for this example. The comparison between the estimated uncertainty and a reference estimate obtained with a Monte Carlo method shows that the uncertainty is not severely reduced during the assimilation as is often the case. The connectivity is successfully reproduced during the iterative procedure despite the rather large distance between the observation points.

## 1. Introduction

The characterization of rock properties is necessary to make reliable numerical predictions of flow and mass transport in the subsurface. Given the sparsity of measurements, geostatistical simulation techniques can be used to obtain multiple realizations of the value of one or more properties over the whole discretized domain while honoring the available measurements. The ensemble of realizations can then be used to quantify the uncertainty of the property, assuming that the variability between the realizations is sufficiently well captured by the ensemble. When these realizations are conditioned to static data only, many realizations often do not reproduce the dynamic flow data. At this stage of the property characterization, the motivation for applying stochastic inverse approaches is to use the available state observations to condition the generated ensemble of geostatistical realizations and thereby reduce the uncertainty. However, as the current trend in hydrogeology is to increase the complexity of the conceptual models with the development of advanced geostatistical techniques, the parameter identification problem using stochastic inverse methods has in parallel also become more challenging.

As underlined by Zhou et al. (2014) for initial non-Gaussian realizations, one drawback of a number of existing inverse approaches is that the reproduced states after the inversion, although in agreement with the observations, are obtained with a loss of consistency: The final realizations depart far too much from the prior geological model. The ensemble Kalman filter (EnKF) introduced by Evensen (1994) and its variants are data assimilation methods, which have drawn particular attention because of their computational efficiency in high-dimensional and nonlinear state and/or parameter estimation problems (Evensen, 2009). However, due to their strong assumption of linearity between the observations and the variables to estimate, these types of algorithms fail to preserve the non-Gaussian structures if they are applied directly to condition a non-multi-Gaussian distribution.

Thanks to an appropriate parameterization, Liu and Oliver (2005) showed that ensemble Kalman methods could be successfully applied even in the more challenging case of categorical simulations generated by truncated Gaussian-based methods. By updating the underlying multi-Gaussian variables instead of the non-Gaussian categorical ones directly, the multi-Gaussian assumption on the variables to update could still be fulfilled, allowing in this way an acceptable performance of the method both in terms of the consistency of the structures characterized and the quality of the data fit achieved.

Among approaches proposed to condition multiple-point statistics (MPS) simulations to dynamic data with ensemble-based Kalman methods, a probability conditioning method was introduced by Jafarpour and Khodabakhshi (2011) in order to derive at each update of EnKF a facies probability map from the ensemble of updated log hydraulic conductivity values, which initially populated categorical MPS realizations of facies. Originally, Jafarpour and Khodabakhshi (2011) proposed to map the mean value computed at each grid block from the ensemble of updated log hydraulic conductivity fields to a probability value by using a linear transformation. Recently, Ma and Jafarpour (2019) proposed an improved approach to derive these probability values by also taking into account the ensemble variance. Either way, the resulting facies probability map was then used as soft conditioning data for the next conditional multiple-point simulation using the MPS algorithm SNESIM (Strebelle, 2002). An interesting outcome of the proposed methodology was that each regeneration of soft-data-conditioned multiple-point simulations following an iteration of EnKF allowed the introduction of some variability in the facies distribution due to the stochastic nature of the MPS method.

The probability conditioning method (Jafarpour and Khodabakhshi, 2011), however, does not attempt to mitigate the effects of the non-multi-Gaussian distribution of log hydraulic conductivities before each update of EnKF. Zhou et al. (2011) proposed a normal-score (NS) transform prior to each computation of the EnKF update so that the ensemble of initial or updated parameter variables is marginally Gaussian in order to reduce the consequences of violating the multi-Gaussianity assumption from the beginning. For their synthetic case, they concluded that such NS transform prior to the update allowed to outperform EnKF without any transformation in terms of the structures that could be retrieved by the end of the data assimilation. It is worth mentioning that their application of the ensemble method was based on an ensemble of 1,000 realizations, which is quite large compared to the standard ensemble sizes of around a hundred of members, and also on an important number of observation points for the hydraulic head data used in the assimilation.

Similarly to the strategy of Liu and Oliver (2005) to condition categorical truncated Gaussian simulations with EnKF via their underlying multi-Gaussian variables, Hu et al. (2013) proposed to apply EnKF to update either the uniform fields underlying the ensemble of categorical MPS realizations generated with SNESIM (Strebelle, 2002) or the coefficients of combination of those underlying uniform fields. Both proposed parameterizations of the MPS simulations have the advantage of allowing the conditioned categorical fields to remain consistent with the prior geological model. Although both allow to deal with continuous instead of discrete parameters, the resulting increased nonlinearity between the parameters to update and the dynamic response ultimately prevented EnKF from reaching a sufficient data match in either case (Hu et al., 2013). Heidari et al. (2013) had also observed a similar lack of flexibility in terms of the final data match achieved when updating gradual deformation parameters with EnKF to perturb an ensemble of multi-Gaussian realizations of a petrophysical property.

Keeping this idea of a parameterization reducing the number of adjustable parameters, Gardet et al. (2014) proposed a multiscale parameterization on the basis of a multi-Gaussian simulation method. The goal was to allow to adapt the scale of the conditioning of parameters according to the data used. Knowing that the finer realizations would be conditioned to the realizations simulated at the coarse scale, an interesting perspective was the possibility of applying at this coarser scale the update from an inverse method. The potential of such strategy was illustrated with the gradual deformation technique.

Mainly motivated by the results of the forementioned studies, this paper introduces a new methodology to condition categorical MPS simulations of facies to dynamic data with an ensemble Kalman method. The workflow relies on a multiresolution parameterization based on generated multiresolution training images (TIs) which allow MPS simulations at coarser resolutions than that of the original TI. The performance of the proposed approach is evaluated using a synthetic 2-D vertical groundwater model and transient hydraulic data at particularly sparse locations in the horizontal direction, as would be the case in many real problems. In this work, the code DeeSse (Straubhaar, 2017), which offers a multiscale parameterization of the direct

sampling (DS) algorithm (Straubhaar et al., 2020) was used. Among existing ensemble Kalman methods, the ensemble smoother with multiple data assimilation (ES-MDA) algorithm (Emerick and Reynolds, 2012) was chosen for its simple formulation and demonstrated efficiency in a real reservoir history-matching problem (Emerick, 2016).

In the next two sections, we first introduce the concepts that are at the heart of the proposed methodology. Section 2 aims to give some background on how the multiresolution MPS simulations are performed in DeeSse. The update algorithm ES-MDA is then presented in section 3. We finally give a walkthrough of the proposed methodology in section 4 based on the previously introduced concepts. The synthetic case including the model setup, the definition of the DeeSse parameters, and the performance criteria is presented in section 5. Finally, the results of the synthetic case are presented and discussed in section 6.

## 2. Multiresolution Multiple-Point Geostatistical Simulations With DeeSse

Since a few decades, the interest for MPS simulations has grown considerably with applications in various fields of geosciences (Mariethoz and Caers, 2015). Given a "TI," an image provided by the user as the conceptual model of the variable to simulate, the goal of MPS is to generate random fields that reproduce the spatial statistics of the TI. Depending on the TI, MPS can render a large variety of geological heterogeneities, including complex connectivity patterns. Among existing MPS algorithms, the DS method (Mariethoz et al., 2010) consists in simulating the nodes of a simulation grid sequentially by directly sampling the TI. For each node to be simulated, the pattern formed by a number of neighboring nodes, either informed by data or which have been previously simulated, is searched in the TI. As soon as the distance measuring the mismatch between the conditioning pattern and the one being currently scanned in the TI is below a given threshold, the corresponding TI value is pasted at the simulation grid location. If no compatible pattern is found after a certain fraction of the TI has been scanned, the search is stopped and the best candidate found so far is used. Hence, the maximal number of neighbors, the distance threshold, and the maximal scanned fraction are the key parameters of an MPS simulation with DS. Besides being computationally efficient, DS offers two advantages of general interest: (1) the ability of handling categorical and continuous variables and (2) the possibility of performing simulations of multiple properties given the multiple-point dependence between given properties (Mariethoz et al., 2012).

DeeSse (Straubhaar, 2017) is an implementation of the DS algorithm with some features allowing to improve the quality of the MPS simulations. Among the recently added features, the "Gaussian pyramid" technique allows to control the simulation at multiple resolutions. The motivation behind this feature was originally to better capture the different scales of heterogeneities that might be present in the TI (Straubhaar et al., 2020). The technique consists in computing coarser versions of a given TI. The resulting set of multiresolution TIs can then be used to perform a series of MPS simulations at different scales, starting from the coarsest scale up to the original scale of the TIs. Those multiresolution MPS simulations establish the multiresolution framework of our proposed data assimilation approach to condition categorical MPS simulations with an ensemble Kalman method presented in section 4. We provide here some background on how such multiscale MPS simulations are performed by DeeSse in the case of a categorical TI.

For a given categorical TI with $N$ categories, the Gaussian pyramid technique creates a pyramid of multiresolution TIs for $N-1$ indicator functions of the different categories. The remaining category is deduced from all the previously simulated ones. Starting from the provided TI, the upscaled images result from the recursive application of a reduce operator on the last image created. As currently implemented in DeeSse, this reduce operator corresponds to the convolution product of the image with a set of Gaussian-like kernels of either 5-pixel width distributed every two nodes in each direction or 7-pixel width distributed every three nodes or a combination of both of these possibilities. Consequently, the spacing of two or three nodes between each kernel will correspond to the reduction factor applied in each direction to the image. By iteratively applying this reduce operator to the last reduced image, one thereby obtains a so-called "Gaussian pyramid" of images. In addition, each reduced image is expanded onto the grid of the next finer scale by assigning first the values in the grid nodes corresponding to the center nodes of the kernel that was used for the reduce operator (one node over two or three depending on the kernel width), and then by computing a moving average, in every node, by using the same kernel with weights normalized over the informed nodes (and ignoring uninformed locations) (Burt and Adelson, 1983). As will be described further below,

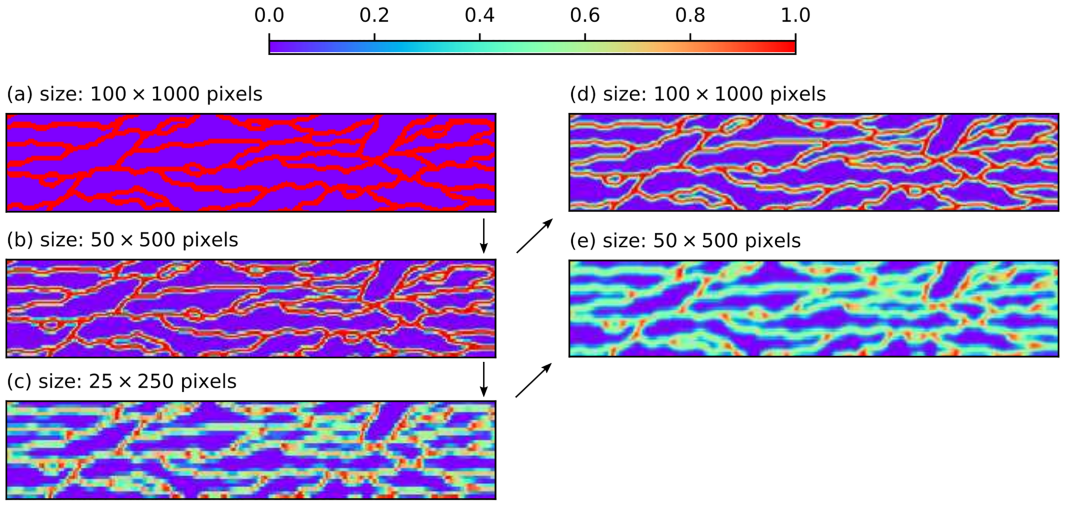


**Figure 1.** Example of a set of multiresolution training images with two additional coarse levels obtained with the Gaussian pyramid technique. A reduction factor of 2 between each level was applied in each direction. Given a categorical training image (a), a first reduced image (b) is obtained. A second reduced image (c) is then obtained from (b). Finally, the images (e) and (d) are created based on the expansion of (c) and (b), respectively.

each pair of expanded and reduced TIs of the same level will allow to perform multivariate MPS simulations (Mariethoz et al., 2012) which are guided by the expansion of the simulation result in the previous coarser-scale grid.

For example, Figure 1 shows for a binary TI the complete set of multiresolution TIs, which will be used at some stage of a series of multiscale MPS simulations performed by DeeSse. As illustrated, this set includes the Gaussian pyramid of TIs obtained for the indicator function of the category of value 1, that is, the channel facies, with two levels of coarse resolutions with a reduction factor of 2 applied in each direction between each level, as well as the pyramid formed by the two expanded images resulting from the respective expansion of the two reduced images. Hence, given both these pyramids of reduced and expanded TIs, an unconditional univariate MPS simulation can first be performed at the coarsest level of the TI pyramid by using the corresponding TI. Then, iteratively, the last coarse simulation is expanded to the next finer

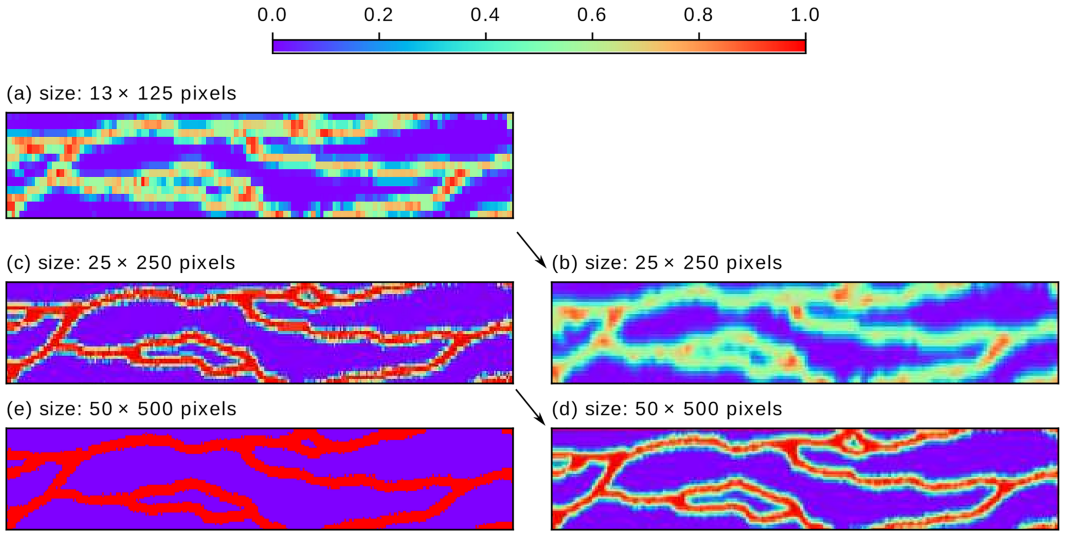


**Figure 2.** Illustration of the multiresolution MPS simulation procedure in DeeSse using the training data set of Figure 1. At the coarsest resolution, a first univariate MPS simulation is generated (a). The simulation is then expanded to the next finer scale of the TI pyramid (b) to guide the next MPS simulation at the finer scale (c) using the corresponding bivariate TI. Again, the last simulation is expanded to the next finer scale (d) and used to guide the categorical MPS simulation (e) using the corresponding bivariate TI.

scale in order to guide, by way of a bivariate MPS simulation, the MPS simulation at that new fine scale using the bivariate TI composed of both the reduced and expanded images of the corresponding level. Based on the multiresolution TIs shown in Figure 1, Figure 2 shows an example of pyramids of multiscale MPS simulations obtained, as well as the expanded images resulting from the coarser-scale simulations, which were used. It is also worth noting that the additional MPS simulations at the coarse scales required with this pyramid option are not necessarily much more time consuming, considering that the number of pixels is reduced from one level of the pyramid to the next coarser one and also as they are guided by the expanded image from the coarser level in the next finer-scale MPS simulation (Straubhaar et al., 2020).

## 3. Ensemble Data Assimilation With ES-MDA

The purpose of this section is to provide some background on the ensemble Kalman method, which was used for the proposed methodology although another variant could be considered. The data assimilation algorithm will allow to update the previously introduced multiresolution MPS simulations and ultimately to condition the categorical facies fields to the observed dynamic data.

### 3.1. General Background

The ES-MDA developed by Emerick and Reynolds (2012) is currently one of the most used ensemble Kalman algorithms for parameter estimation in reservoir applications (Evensen, 2018; Abadpour et al., 2018). The algorithm consists in repeating the ES update equation, for each parameter realization $m_i$ where $i = 1, 2, ..., N$ with $N$ the ensemble size, a predefined number of times $k$

$$m_i^{k+1} = m_i^k + C^k{}_{\mathrm{MD}}(C^k{}_{\mathrm{DD}} + \alpha_{k+1}C_{\mathrm{err}})^{-1}(d^k{}_{\mathrm{obs},i} - g(m_i^k)), \tag{1}$$

where $C^k_{\mathrm{MD}}$, the cross-covariance matrix between the parameter vector $m_i$ and the vector of predicted data $g(m_i)$, and $C^k_{\mathrm{DD}}$, the autocovariance matrix of predicted data, are approximated from the ensemble at iteration $k$. Compared to ES, the covariance matrix of the measurement errors $C_{\mathrm{err}}$ is in ES-MDA purposely inflated by a factor $\alpha > 1$ to limit the confidence given to the data as they will be assimilated multiple times. As a result, the observed data $d^k_{\mathrm{obs},i}$ used to compute the residuals in the update equation (1) are the actual measurements $d_{\mathrm{obs}}$, which have been perturbed with a Gaussian noise sampled at each iteration from an inflated covariance of measurement errors $\alpha_{k+1}C_{\mathrm{err}}$ as follows:

$$d^k_{\mathrm{obs},i} = d_{\mathrm{obs}} + \sqrt{\alpha_{k+1}}C^{1/2}_{\mathrm{err}}z_i, \tag{2}$$

where $z_i$ is a vector of standard normal deviates; that is, $z_i \sim N(0, I)$. Hence, at each new iteration $k + 1$, each updated realization $m_i^{k+1}$ is computed as the linear combination of the updated realization $m_i^k$ of the previous iteration $k$ and each component of the vector of residuals between $d^k_{\mathrm{obs},i}$, the vector of observed data to assimilate, and $g(m_i^k)$, the vector of corresponding predicted data from the nonlinear forward model $g$. For each component of the ensemble of parameter vector realizations $m_i^k$, each residual is then weighted on the basis of the Kalman gain matrix $K$ computed from the ensemble of realizations $m_i$ as

$$K = C^k_{\mathrm{MD}}(C^k_{\mathrm{DD}} + \alpha_{k+1}C_{\mathrm{err}})^{-1}. \tag{3}$$

Iterative ES algorithms such as ES-MDA aim to handle iteratively potential nonlinearities between the parameters and the assimilated data, so that ultimately a better fit of the data can be achieved than when using noniterative methods. ES-MDA was in fact developed so that it would be comparable to several iterations of the Gauss-Newton optimization procedure (Emerick and Reynolds, 2012). Since the use of multiple iterations in such a procedure allows to compute smaller and more accurate updates than one single potentially large and less accurate iteration, a more efficient reduction of the objective function being minimized is expected after the iterations of ES-MDA than after the single iteration of ES in nonlinear problems (Evensen, 2018).

To test the proposed methodology to condition categorical MPS realizations presented in section 4, we will use the standard implementation of ES-MDA (Emerick and Reynolds, 2012) and set, for simplicity, constant inflation coefficients equal to the predefined number of assimilations. Indeed, no matter the implementation of ES-MDA used, all the factors $\alpha_k$ used to inflate the observations assimilated by ES-MDA should satisfy the following condition:

$$\sum_{k=1}^{N_a} \frac{1}{\alpha_k} = 1, \tag{4}$$

where $N_a$ is the number of times we repeat the data assimilation. This condition was derived to ensure the equivalence between the single ES update and the iterative ES-MDA for a linear Gaussian case (Emerick and Reynolds, 2012).

### 3.2. Localization and NS Transform

Ensemble Kalman methods are generally implemented along with ad hoc methods designed to mitigate their intrinsic deficiencies, thereby getting the best possible performance out of them. Hereinafter, the purpose of two mitigation methods is stated since they will both play a significant role in the proposed methodology to condition categorical multiple-point realizations presented in section 4.

A major limitation of EnKF and other variants such as ES-MDA is that the finite size of the ensemble can introduce undersampling errors in the covariance matrices approximated from the ensemble (Houtekamer and Mitchell, 2006). In particular, "spurious" long-range correlations between components of the parameter vector and the predicted data can occur and bring an undesirable response in both the updated mean and covariance. At worst, they can reduce the parameter variance to the point where the covariance of the updated ensemble can collapse, thereby wrongly increasing the confidence in certain parameters and, as a result, preventing the successful assimilation of data that could contribute significantly to the parameter identification.

The tapering of the sample covariances, also referred as "covariance localization," is a method widely used to filter out those undesirable correlations. For our application of ES-MDA, we will apply a standard approach, which consists in restricting the magnitude of the update computed close to the observation locations by using a tapering function. The Kalman gain matrix (3) will be attenuated by multiplying each one of its entries by a localization factor between 0 and 1. This localization is often defined as a function of the physical distance between each couple of parameter and data variables. An example of common forms used for this function is the fifth-order correlation function with compact support as defined by Gaspari and Cohn (1999). We will use this function since it has been used for many applications where localization in the horizontal direction is important (Anderson, 2012), as in our synthetic case presented in section 5. Note that to evaluate this function, a "critical length" that corresponds to the distance beyond which the localization factor will rapidly decrease to 0 needs to be defined initially.

Another important and more general limitation of ensemble Kalman methods is their underlying assumption of multivariate normal distributions. Because the Kalman gain is based only on the evaluation of covariance matrices, the update performed by all these types of methods will only be able to take into consideration the linear dependence between the variables. As a result, the statistics of order higher than 2 of an initial ensemble of realizations generated by MPS, for example, would not be preserved after the update, and neither the potential initial non-Gaussian structures.

To deal with non-multi-Gaussian ensembles, Zhou et al. (2011) proposed to perform the update in such a way that every marginal distribution is Gaussian. As illustrated in Zhou et al. (2011), for each parameter variable at every location, a NS transform function is defined such that the $p$-quantile of the ensemble distribution of original values is mapped to the $p$-quantile of a standard normal distribution. After the update is performed on these transformed parameter variables, they need to be back-transformed to be able to run the forward model and predict the corresponding new observations. Although this approach has shown to improve the estimates of the ensemble Kalman method if supported by enough spatially distributed data (Li et al., 2012; Zovi et al., 2017), it is important to note that this parameter transformation only mitigates and hence does not completely solve the problem related to updating non-multi-Gaussian variables. Indeed, dealing with Gaussian marginal distributions does not necessarily imply a joint Gaussian distribution for all the variables. It is also worth reminding that the NS transform approach could be applied until now, in the context of conditioning of MPS simulations with ensemble Kalman methods, because the parameters were values of a continuous property, such as log hydraulic conductivities, and not categorical values, such as for geological facies. For categorical variables, it would not be possible to define such NS transform. As the proposed methodology presented in the next section aims to condition categorical MPS simulations, the idea will be to update, in the same manner as Zhou et al. (2011), continuous parameters. As will be further explained, those continuous parameters will be defined at a coarser resolution than the resolution of

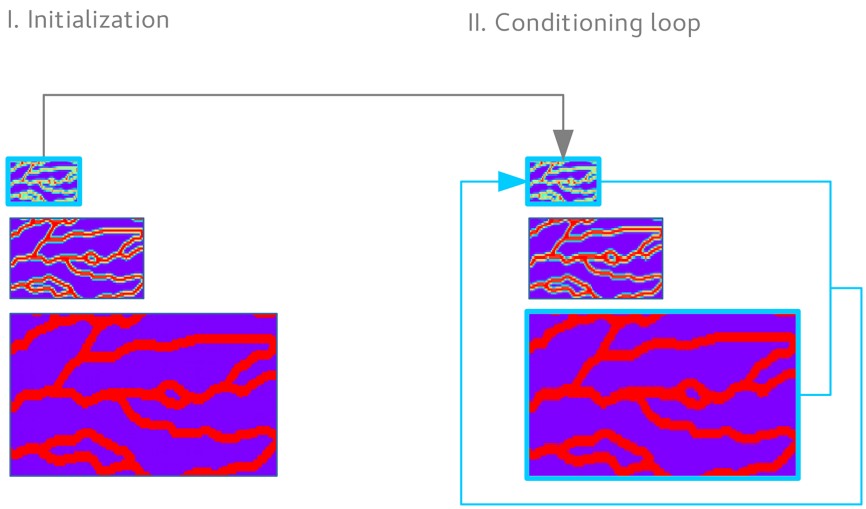


**Figure 3.** Overview of the procedure to condition categorical multiple-point simulations with ES-MDA using a multiresolution parameterization. For each ensemble member, (I) a multiresolution MPS simulation is generated and the image of the coarsest level (i.e., with the smallest size) is extracted. (II) The coarsest-resolution parameters are used to condition the categorical MPS simulation. Both the ensemble of coarsest-resolution parameters and categorical fields are involved in the computation of the update for the current iteration.

the categorical MPS simulation. Moreover, those parameters will be more directly related to the categorical variables thanks to the multiscale framework for data assimilation established by the multiresolution MPS simulations.

## 4. ES-MDA With Multiresolution MPS Simulations

This section aims to describe how the multiresolution MPS simulations with DeeSse and the ES-MDA algorithm are combined together to yield the proposed methodology.

### 4.1. Obtaining the Latent Variable

As previously introduced in section 2, a multiresolution MPS simulation provides a straightforward way to relate the categorical MPS simulation to a latent continuous variable at a coarse scale. The ES-MDA update can then be applied on the latent continuous variable instead of the categorical variable. Therefore, the first step of the proposed methodology consists in extracting the coarsest-resolution MPS simulation for each member of an ensemble of multiresolution MPS simulations performed with DeeSse. It is worth mentioning that if hard conditioning data are provided for the categorical MPS simulation, these data would first be propagated through the different coarse levels of the pyramid before performing the series of MPS simulations (Straubhaar et al., 2020).

An immediate consequence of choosing the coarse image for the parameterization is a massive reduction of the number of parameters to update with ES-MDA. The number of parameters will ultimately depend on the number of pyramid levels and the size of the Gaussian kernels applied in each direction for each level. A second consequence of the proposed parameterization comes from the process of the TI reduction itself. The coarse MPS simulation will be a coarse version of the fine categorical MPS simulation, even though the former is simulated first as described in section 2. As shown in Figure 2, the coarse simulation will present smooth instead of sharp transitions between the facies. Considering that ensemble Kalman methods such as ES-MDA are not suitable for directly updating fields containing discrete features, it is expected that the blurring effect affecting the simulated structures at coarse resolutions will benefit the performance of the method.

### 4.2. Conditioning the Categorical Field

To assimilate the state variable observations, the computation of the ES-MDA update requires to compute the flow model response associated to the parameters, which are going to be, or are already, updated. For this purpose, the same hard conditioning procedure, which is at the heart of the multiresolution MPS simulation, as described in section 4.5, can be employed to derive a categorical MPS simulation conditioned to

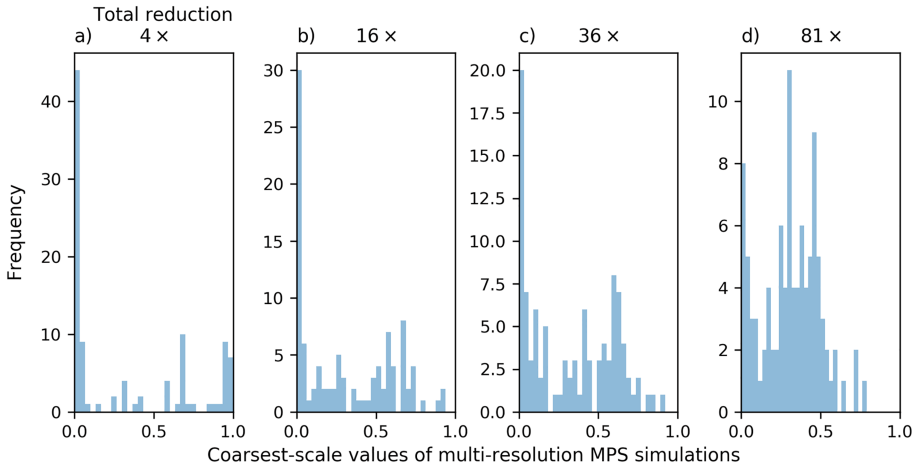


**Figure 4.** Distribution of values at a random location from an ensemble of coarsest-resolution MPS simulations for four different resolutions (a)–(d). For all cases, the size of the original (finest) binary simulation is 50×500 pixels. (a) 25×250 (reduced once with a factor 2 in each direction), (b) 13 × 125 (reduced twice with a factor 2 in each direction), (c) 9 × 84 (reduced first with a factor 2 in each direction, reduced again with a factor 3 in each direction), and (d) 6 × 56 (reduced twice with a factor 3 in each direction). The distribution becomes increasingly smoother as the resolution decreases.

the coarsest resolution parameters. The categorical field can then be conveniently used for the flow simulation, after assigning petrophysical property values to each category of facies. Once all the flow simulations of the ensemble are completed, the update of the coarsest-resolution variables can be computed based on the covariance matrices estimated from both the ensembles of coarse parameters and simulated flow data. An overview of the conditioning procedure is illustrated in Figure 3.

Note that, although they are not shown in Figure 3, two additional preprocessing steps are included in the final methodology proposed and are described in the next sections. They aim to mitigate the limitations which inevitably arise when the multi-Gaussian requirement on the initial ensemble is not met.

### 4.3. NS Transform

We compute a NS transform function for each pixel of the coarsest resolution fields of the initial ensemble. Indeed, Figure 4 shows that the distribution for the ensembles of coarsest-scale MPS simulations generated using different settings of pyramid parameters have marginal distributions that are not Gaussian. This figure also shows that the local distributions are getting closer to normal when the number of levels increases. By applying each NS transform locally, we ensure that every marginal distribution becomes Gaussian. The ES-MDA update will then be applied on the transformed variable rather than on the images coming directly from the pyramid of MPS simulations, as illustrated in Figure 5. Note that the computation of local NS transforms is performed only once before the whole iterative process with ES-MDA.

As mentioned in the previous section, the conditioned categorical fields will be obtained from the coarsest resolution according to the same hard conditioning procedure allowing to generate a multiresolution MPS simulation. Therefore, the updated transformed variables will need to be back-transformed in order for the values to be consistent with those of the coarsest-resolution TI, that is, between 0 and 1. For this reason, we will apply on the ensemble, after each update, a back NS transform function at every location. This function corresponds to the inverse function of the NS function previously used. When applying the back NS function, we also ensure that the back-transformed values will be bounded between 0 and 1 by not allowing extrapolation for values falling outside the domain of the function.

### 4.4. Sampling and Final Parameterization of the Multiresolution MPS Simulations

Given that ensemble Kalman methods are known to break the prior structures after an update, we do not fully inform the coarsest resolution of the multiresolution MPS simulation with the complete back-transformed image as hard data. Instead, only a set of values at selected locations of the back-transformed image will be considered as hard conditioning points. Those locations should be as distributed as possible over the whole model domain so that DeeSse can still simulate in between them and in this way recover more consistent structures. The highest the number of nonadjacent locations, the better in

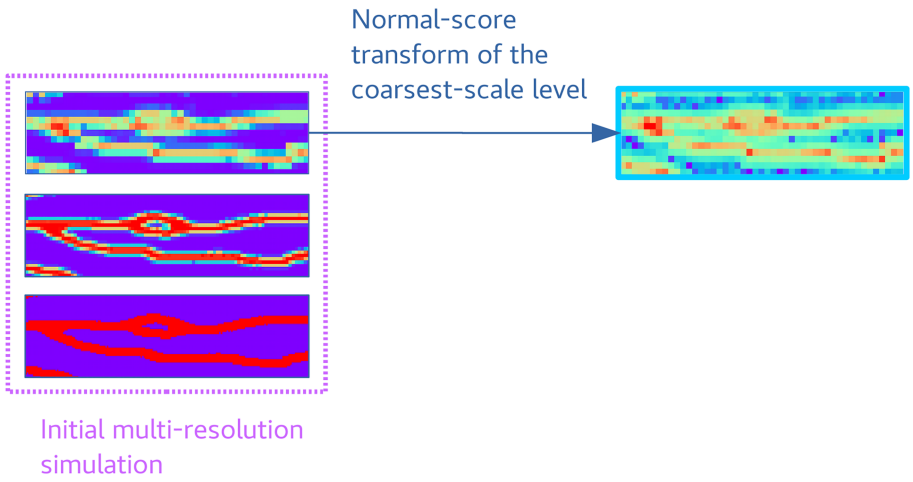


**Figure 5.** Illustration of the normal-score transform step performed for each member of an initial ensemble of multiresolution MPS simulations before the conditioning.

order to efficiently constrain the data match. Ultimately, DeeSse will simulate a complete pyramid starting by a conditional simulation at the coarsest scale.

As can be observed in Figure 6, using conditioning points instead of a conditioning image will effectively prevent DeeSse to pass on the finer-scale MPS simulations the degraded structures of the whole updated field. Therefore, the update of ES-MDA is integrated only locally at the coarsest resolution of the MPS simulation and then indirectly to the subsequent finer ones via the expansion of the last MPS simulation and its use as a fully informed hard conditioning image for the following scale. Figure 6 illustrates the benefit of the sampling process and its integration at the coarsest scale of the multiresolution MPS simulation.

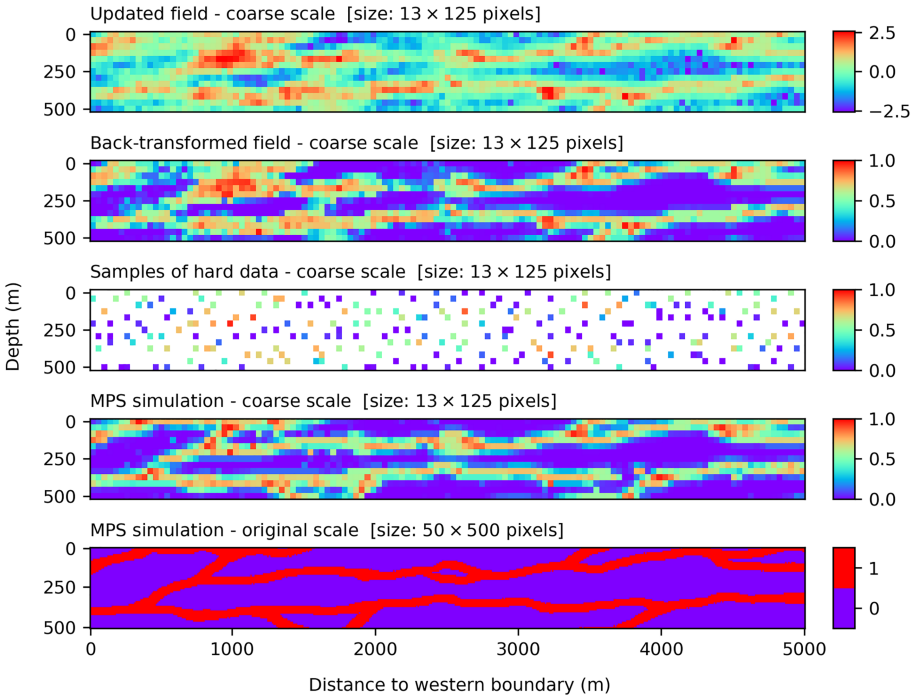


**Figure 6.** Conditioning a categorical MPS realization (bottom image) from the updated normal-scored image at the coarsest pyramid scale (Ensemble Member No. 11) at iteration 8 out of 16 of ES-MDA (top image) via the fixedly sampled back-transformed image used initially as hard conditioning points for the multiresolution MPS simulation.

In addition, the sampled hard conditioning points over the whole domain offers a way to prevent expected discontinuous transitions at every scale of the MPS simulations when localizing the update of the parameters close to the observations. This is in fact illustrated in Figure 6 where only the region located up to around $x = 1,600$ m from the western boundary is being updated due to the locations of the observations only in this region of the model. As can be observed, the structures simulated by MPS after each update, first at the coarsest and ultimately at the original scale, remain continuous at the transition between the updated and nonupdated parameters at $x = 1,600$ m.

The conditioning of the categorical field in the proposed methodology relies on a series of MPS simulations performed at every scale of a generated set of multiresolution TIs. This implies that a high degree of randomness will be introduced in the relationship between the coarse parameters and the flow data calculated from the conditioned categorical field.

For the application of the ensemble Kalman method, it is critical to establish a forward operator that ensures (1) the derivation of a unique categorical field given a set of coarse parameters and (2) a derivation which is obtained in a systematic manner for all members of the ensemble. Otherwise, the estimated covariance matrices will not be reliable for the computation of the updates. For both these above-mentioned reasons, an important first prerequisite is that the hard conditioning points should be sampled from the same locations for all ensemble members and for all iterations of ES-MDA. Then, the second and most decisive prerequisite is that the same seed number for the multiresolution MPS simulations should be used for all iterations and for all ensemble members.

For one ensemble member and given the same locations of hard conditioning points for all iterations, a same seed value allows the reproducibility of the multiresolution MPS simulation if the values at the hard conditioning points are the same. By extending for all ensemble members and for all iterations, both these conditions on the same locations of the hard conditioning points and the same seed value, we allow the ensemble of multiresolution MPS simulations to be performed in a systematic manner. Indeed, provided that the locations of the hard conditioning points at the coarsest scale are the same for all members, using the same seed will make DeeSse simulate the ensemble of coarsest-scale MPS simulations by using the same randomly generated simulation path. A same path for all ensemble members will also be used for the subsequent ensemble of finer-scale simulations. In this manner, the forward operator established will be sufficiently systematic for the ensemble Kalman method to capture and exploit the relationship between the parameters and the data, and this in spite of the intrinsic randomness of the parameterization with multiresolution MPS simulations.

Moreover, the use of the same seed value for all the ensemble members means that the variability between the ensemble members will entirely be controlled by the variability of the values at hard conditioning points which are updated by ES-MDA. Therefore, we will be certain that a successful convergence of the proposed methodology will be mostly on account of the performance of the update algorithm rather than the randomness of the DeeSse simulations.

The question of the number of hard conditioning points to use is case dependent, and hence, we cannot draw general conclusions based only on our synthetic case study. However, the optimal number will depend on the multiresolution parameterization defined, that is, the number of pyramid levels and the reduction factor applied in each direction of the TI for each level. In general, the pyramid parameters should depend on the largest size of the structures we wish to simulate. In the context of the proposed methodology, the idea is to ensure that the structures at the coarsest scale will be discernible with the lowest resolution possible so as to mitigate the expected discontinuities after each ES-MDA update of a non-multi-Gaussian distribution. Indeed, such a multiresolution parameterization, alone, will allow to alleviate those consequences thanks to the resulting more continuous distribution at the coarsest scale. Since the continuity of the structures will be, in this manner, less compromised after an ES-MDA update, the optimal number of points will be allowed to be significantly higher than in a case without such a multiresolution parameterization. However, it is important that the hard conditioning points are distributed evenly instead of being clustered. This way, DeeSse can play its role of retrieving the connectivity between the points according to the compatible patterns found in the TI, as shown in Figure 6. We will further address the benefit of the multiresolution parameterization on the number of hard conditioning points when discussing the results obtained on our synthetic case in section 6.

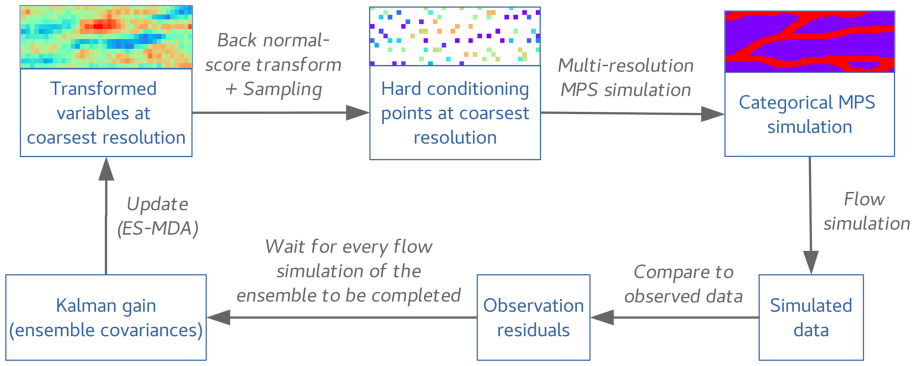


**Figure 7.** Workflow for each ensemble member to condition the categorical MPS simulations with ES-MDA. The multiresolution simulations are regenerated based on updated parameters at the coarsest scale.

### 4.5. Complete Procedure

To summarize, the proposed algorithm proceeds as follows. We start from the NS transformed variables obtained from the initial ensemble of coarsest-resolution MPS simulations, as illustrated in Figure 5. Then, Figure 7 illustrates the complete conditioning procedure for each ensemble member. The method includes the back-transform and sampling steps before the local integration of the ES-MDA update at the coarsest scale of the multiresolution MPS simulation.

It is worth noting that the sampled hard conditioning points are ultimately the only points affecting the simulated categorical fields. Therefore, the sampling could be in fact performed before the NS transform step. In this manner, only the sampled transformed variables would be updated before being back-transformed as hard data for the multiresolution MPS simulation. However, for the sake of illustrating the motivation behind the sampling step, we purposely kept the description of the complete algorithm in this order.

## 5. Synthetic Test Case

A synthetic numerical experiment is conducted to evaluate the performance of the proposed method. The model is inspired by the artificially induced flow resulting from the excavation of vertical shafts. The hydraulic impact of such perturbation has, for example, been monitored and studied at the Andra's Meuse/Haute-Marne since the operation of the Underground Research Laboratory (Benabderrahmane et al., 2014; Deman et al., 2015; Kerrou et al., 2017).

### 5.1. Model Setup

The domain is two-dimensional and covers a vertical section of rectangular shape of 5,000 m along the east-west direction and 500 m in depth. It represents a section of the Oxfordian limestone multilayered aquifer above the Callovo-Oxfordian clay host formation, which is not included in the model. For groundwater flow computation, the domain is discretized by 50 × 500 square elements of 10 m wide.

Along the top boundary, constant heads are imposed. The head values vary linearly between 267.5 m on the west side and 284 m on the east side. At depth, between 150 and 500 m, a prescribed head of 280 m is imposed on the east side to maintain a continuous east-west flow in the system (Figure 8). In order to

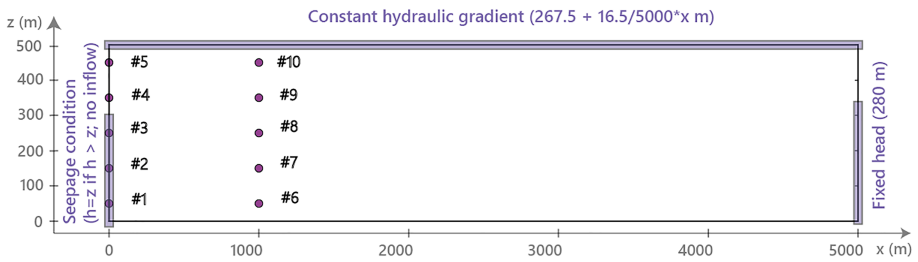


**Figure 8.** The two-dimensional vertical domain modelled of 5,000-m length and 500-m depth. The thin rectangles indicates the location of nodes with a boundary condition applied. The dots indicates the head observation nodes. Not shown here, the left boundary is divided into five zones where the flow rates are observed.

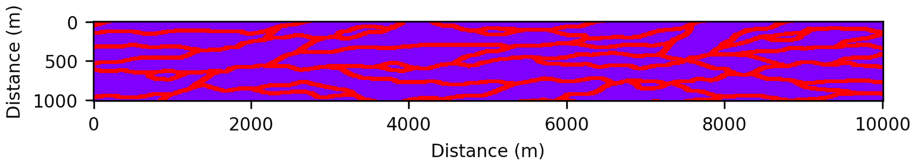


**Figure 9.** Binary training image of size $1,000 \times 100$ pixels used to generate the multiple-point simulations with DeeSse. It is the same categorical TI for which an example of set of multiresolution training images was shown previously in Figure 1.

mimic the type of hydraulic perturbation created by a vertical shaft, a subsequent transient flow simulation is calculated by adding from time zero, in addition to the boundary conditions previously listed, a seepage condition over the nodes corresponding to the first 300 m of the western boundary starting from the bottom (Figure 8). We assume that the nodes over the remaining 200 m towards the surface are not affected as we suppose that they are associated to an isolated upper part of the shaft. Note that in exploratory simulations, a sensitivity analysis was carried out on different levels of the finite element mesh refinement and the solver parameters, as well as on various types of flow boundary conditions and hydraulic property values. This was done in order to ensure robust numerical solutions and also to avoid bias from boundary effects.

For simplicity, the groundwater flow equation was solved numerically under saturated conditions. All the groundwater flow simulations in the framework of this study were performed with the simulator Ground-Water (Cornaton, 2014). This numerical code uses the standard Galerkin finite element and the control volume finite element methods and has been validated on the basis of a series of standard benchmarks by comparison with analytical solutions as well as with commercial numerical simulators.

### 5.2. Synthetic Data Set

The reference parameter field is a categorical MPS realization generated with DeeSse using the $100 \times 1,000$ pixel binary TI shown in Figure 9. It represents the distribution of two geological facies in the domain. The TI was obtained using the $2,500 \times 2,500$ hand drawn image by Zahner et al. (2016) inspired by Strebelle (2002). Before extracting our $100 \times 1,000$ TI from this forementioned image, we first resized its first dimension so to have more than one channel simulated on the vertical direction of our $50 \times 500$ simulation grid. The TI for our test case was chosen 4 times bigger than the size of the simulation grid used to simulate the categorical MPS realizations in order to ensure sufficient variability between the initial unconditional realizations.

To simulate the groundwater flow, each category of facies was populated with hydraulic properties. An initial steady state flow before the activation of the seepage boundary condition was first computed by assuming constant values of hydraulic conductivity of $10^{-4}$ m/s for the channels and of $10^{-6}$ m/s for the less permeable matrix. For the subsequent transient groundwater flow simulation, the specific storage was set to a constant value of $10^{-6}$ $m^{-1}$ over the whole domain. The transient flow was computed over a duration of 43,200 s so that the expected decrease of hydraulic heads at the observation locations shown in Figure 8 can be well captured. Hence, the drawdown is locally monitored in 10 locations at five different depths every 100 m. The first points are located along the seepage vertical boundary and the second ones at 1,000 m from the first. The simulated heads were collected every 1,200 s from $t = 0$ s to $t = 43,200$ s, hence at 37 time steps. The resulting flow rates produced at the seepage western boundary were also measured, but at a smaller constant time step of 300 s for five zones of nodes spread along the boundary. To test the methodology proposed in section 4, we will consider the ten time series of simulated hydraulic head as the data for the assimilation. The five flow rate data time series will then be used in addition in order to test the flow predictions obtained. For this inverse problem, we assume that the uncertainty related to the built groundwater flow model is negligible compared to the uncertainty on the facies distribution.

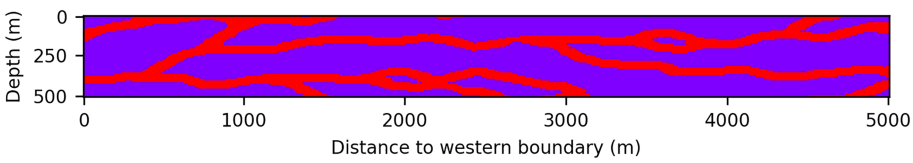


**Figure 10.** Reference Field A of size $50 \times 500$ pixels corresponding to a multiple-point realization of the training image.

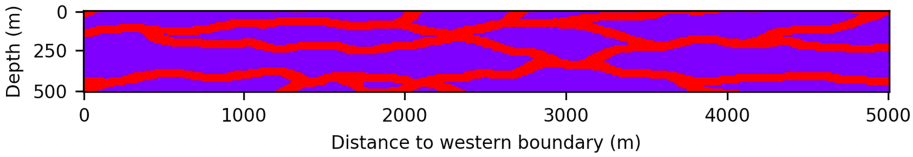


**Figure 11.** Reference Field B size 50 × 500 pixels corresponding to a multiple-point realization of the training image.

To test the performance of the methodology, we considered in this study two different reference fields of the facies distribution named "A" (Figure 10) and "B" (Figure 11). They differ by the extent of the drawdown region obtained by the end of the transient flow simulation ($t = 43,200$ s) as illustrated in Figures 12 and 13. Indeed, the drawdown simulated in the Case B goes around a hundred of meters further away from the western seepage boundary than the drawdown simulated with the Reference A. This implies that the synthetic data set relative to the Reference B is sensitive to a broader region of parameters as compared to the Reference A.

### 5.3. Generation of the Multiresolution TIs With DeeSse

To generate the multiresolution TIs, the parameters of the Gaussian pyramid technique, that is, the number of levels and the number of nodes between each Gaussian-like kernel applications, were defined in such a way that the edges of the structures at the coarsest resolution of the pyramid would be as much blurred as possible while still being discernible. As shown by Figure 4, the almost uniform marginal distribution of the MPS simulations below a certain coarse resolution prevents to still detect the structures.

For the categorical TI in our synthetic case, if the most reduced image is only 4 times smaller than the original scale, as shown by the first level in Figure 1b, the image still appears more discrete than continuous. As a result of this still high resolution compared to the size of the structures in the resulting coarse simulations, the strong deviation from the multi-Gaussian assumption (Figure 4a) will likely cause the ES-MDA update to break the initial structures even after having applied beforehand the NS transform. In contrast, if the reduced image is 36 or 81 times smaller, the size of the pixels becomes too large to still detect the structures. In the end, a TI pyramid with two coarse levels and Gaussian-like kernels applied every two nodes was generated (Figure 1). The coarsest scale of the multiresolution MPS simulations is 13 × 125 pixels, hence 16 times smaller than the original size of 50 × 500.

### 5.4. Initial Ensemble of Parameters and Assumptions for the ES-MDA Update

The initial ensemble of NS transformed parameters was obtained from the coarsest-scale simulations of an ensemble of 100 multiresolution MPS simulations. Since only a subset of the 1,625 grid blocks at the coarsest resolution will be taken into account to condition the multiresolution MPS simulation for each ensemble member, using an ensemble of 100 members seems acceptable to approximate the covariance matrices involved in the computation the ES-MDA update. Even though a categorical MPS simulation was initially obtained from the coarsest-resolution MPS simulation, we remind that this categorical field is not the one used to compute the first update of ES-MDA. It is the one simulated from the initial member of parameters according to the forward operator established in the conditioning procedure (Figure 7) that will be used to ensure a consistency between all the updates.

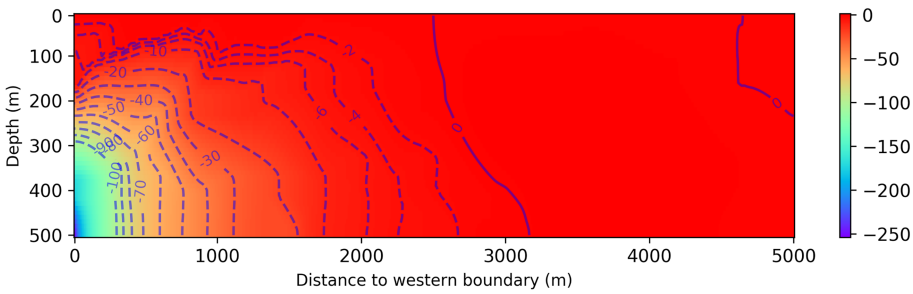


**Figure 12.** Drawdown (m) computed at the end of the transient groundwater flow simulation ($t = 43,200$ s) using the Reference Field A.

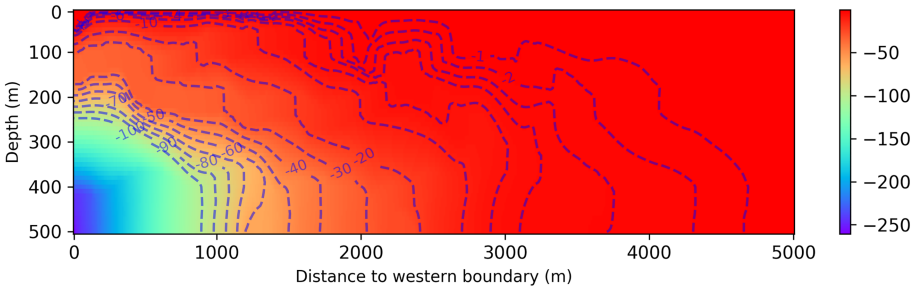


**Figure 13.** Drawdown (m) computed at the end of the transient groundwater flow simulation ($t = 43,200$ s) using the Reference Field B.

A diagonal covariance matrix of independent measurement errors of 0.05 $m^2$ for every head observation was defined. A critical length of 1,600 m, hence almost twice the distance between the two series of observation points at $x = 0$ m and $x = 1000$ m, was defined to localize the Kalman gain matrix on the basis of the Gaspari-Cohn function. By doing that, we are assuming that the estimated covariance between one parameter and an observation located beyond the defined critical length is too noisy to be trusted for the computation of the parameter update. As mentioned in section 3.2, the contribution from these observations will not be considered in the parameter update by applying the forementioned distance-based localization. As a matter of fact, we defined this distance in such a way that the parameters located outside the perturbed area would not be updated (Figure 12). Note that this perturbed area is known precisely here only because we could simulate the flow over the whole domain knowing the reference field. In a real application, we would expect to have a similar knowledge of the extent of the hydraulic perturbation, but with much higher uncertainty.

### 5.5. DeeSse Parameters for the Multiresolution MPS Simulations

We show in Table 1 the parameters of DeeSse used to generate the multiresolution MPS simulations for our synthetic case. For the "Initialization" step, that is, when the initial ensemble of multiresolution MPS simulations is created, the seed value was set to be different for each ensemble member. This way, the MPS simulations are ensured to be different from each other. The maximal scan fraction was also set to 0.25 in order to ensure a sufficient variability in the initial ensemble of coarsest-resolution MPS simulations before the data assimilation. During the conditioning with ES-MDA, the seed was set to be the same value for all ensemble members and for all iterations in order to have a properly defined forward operator especially during the multiresolution MPS simulation as explained in section 4. As a matter of fact, it is possible to adjust the key parameters of DS, that is, number of neighbors, distance threshold, and maximal scan fraction, according to the level of the pyramid in a multiresolution MPS simulation. For every level, we set the number of neighbors to 64 and the distance threshold to 0.05, both of which being in agreement with recommended parameters for MPS simulations with DeeSse (Meerschman et al., 2013). As for the maximal scanned fraction, knowing that the size of coarser simulation grids is much smaller, we could afford to set at both coarse levels a high value of 0.8, hence 3 to 4 times greater than the more standard value of 0.25 defined for the original-scale MPS simulations.

**Table 1**
*DeeSse Parameters Used for Multiscale MPS Simulations in the Proposed Conditioning Approach for Categorical MPS Realizations With ES-MDA*

| DeeSse parameters for multiscale MPS simulations | Initialization | Conditioning loop |
|---|---|---|
| Seed | From 777 to 876 | 999 |
| Number of neighbors | 64 | 64 |
| Distance threshold | 0.05 | 0.05 |
| Maximal scan fraction at Level 2 (coarsest scale) | 0.25 | 0.8 |
| Maximal scan fraction at Level 1 (intermediate coarse scale) | 0.25 | 0.8 |
| Maximal scan fraction at Level 0 (original scale) | 0.25 | 0.25 |

### 5.6. Performance Assessment Criteria

In this section, we present the quantitative criteria used for assessing the performance of the proposed methodology on our synthetic case. In particular, these criteria aim to inform about how the approach deals with the issues often encountered when applying ensemble Kalman methods to condition non-multi-Gaussian realizations. They will allow us to address the quality of the data fit achieved, the plausibility of the categorical fields, and the accuracy of the estimated uncertainty.

Considering that the multiresolution parameterization involves the regeneration of a multiresolution MPS simulation after each iteration of ES-MDA (Figure 3), it is expected that the variability introduced by the MPS simulations at every scale will make the iterative reduction of the data mismatch more challenging. Checking the convergence of the reduction of the data mismatch over the ES-MDA iterations should therefore be the first indication as to the success of the proposed methodology. To evaluate the mismatch between the simulated and observed data, we will compute the sum of the squared deviations between the simulated data and observations normalized by the measurement error standard deviation.

$$D(m_i) = (g(m_i) - d_{\text{obs},i})^T C_{\text{err}}^{-1}(g(m_i) - d_{\text{obs},i}). \tag{5}$$

Even if the reduction of the data mismatch over the iterations turns out to converge to a sufficiently low final value for every final conditioned categorical MPS realization, the geological realism of the facies fields is not guaranteed throughout the inversion procedure using ES-MDA. Given their assumption of multi-Gaussianity, ensemble Kalman methods are indeed expected to "Gaussianize" any type of prior distribution. For this reason, perhaps the most important performance criteria for the assessment of the approach will be those checking the consistency of the final categorical MPS realizations of facies in comparison to the ones obtained initially before the conditioning. For this purpose, we will compute the connectivity function (Renard and Allard, 2013) of the facies of value $s_i$, noted $\pi_i(h)$,

$$\pi_i(h) = Prob\{x \leftrightarrow x + h | s(x) = s(x + h) = s_i\}, \tag{6}$$

which describes the probability that two points separated by a distance $h$ of the same facies of value $s_i$ are connected (6). We will compute it before and after the data assimilation for the facies of value 1, which represents the channels in our case.

In most applications, ensemble Kalman methods may significantly underestimate the true uncertainty of the estimated variables (Chen and Zhang, 2006). We assume that this underestimation would be even greater if the prior distribution is not multi-Gaussian. A main concern when applying an ensemble Kalman method is therefore to obtain a proper estimate of the reduced uncertainty, or in other words, one which is not too much overreduced. Based on the initial and updated ensembles of facies realizations, the uncertainty reduction can be quantified for each facies by observing the variability of the ensemble of facies indicator fields during the assimilation. This variability can be measured by calculating the spatially averaged uncertainty estimated from the ensemble of indicator fields, also known as the "ensemble spread" as follows:

$$S_{\text{ens}} = \sqrt{\frac{1}{N_m}\sum_{i=1}^{N_m}\sigma_{\text{ens},i}^2}, \tag{7}$$

where $\sigma_{\text{ens},i}^2$ denotes the variance at one grid block $i$ from the ensemble of indicator realizations.

To check the accuracy of the uncertainty reduction estimated by ES-MDA in the proposed methodology, we will compare the ensemble spread to the root-mean-square error (RMSE), which measures the discrepancy between the ensemble mean of the facies indicator realizations and the reference facies indicator field as follows:

$$RMSE = \sqrt{\frac{1}{N_m}\sum_{j=1}^{N_m}(m_{\text{true}}^j - m_e^j)^2}, \tag{8}$$

where $N_m$ is the number of grid blocks, $m_{\text{true}}^j$ is the value at node $j$ in the reference facies indicator field, and $m_e^j$ is the value at node $j$ of the mean of the ensemble of facies realizations. The RMSE can then be

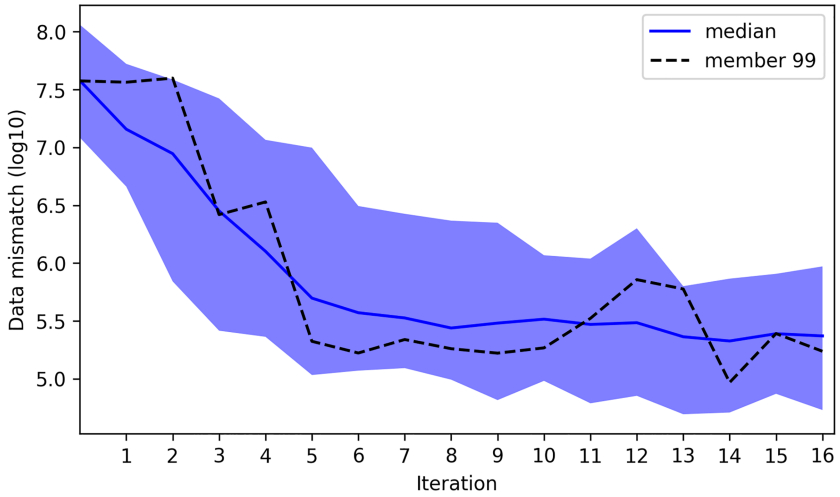


**Figure 14.** Evolution with the iterations of the decimal logarithm of the data mismatch for the test case with Reference A. The solid blue curve is the median, the blue area corresponds to the region between the Percentiles P5 and P95 of the ensemble of values, and the dashed black curve is the values computed for the Ensemble Member No. 99.

calculated based on the initial ensemble of facies realizations generated initially and based on the ensembles of conditioned categorical fields obtained after each ES-MDA update. If the uncertainty is properly estimated during the data assimilation, the ensemble spread should be close to the RMSE (Chen and Zhang, 2006). Indeed, an uncertainty reduction estimated by the ensemble should normally translate into a reduction, of the same magnitude, of the discrepancy between the ensemble mean of facies indicator realizations and the reference. Note that both the ensemble spread and RMSE are both unitless since we are considering either the indicator variables, their mean, or their variance.

Assuming that the amount of information provided by the data is sufficient, the performance of the proposed methodology could also be assessed by its ability to obtain facies realizations that are closer to the reference than before the assimilation. To measure this, we can consider a RMSE defined differently from previously, noted $RMSE_2$, which would here consider the discrepancy, on average, of the reference with each facies indicator realization as follows:

$$RMSE_2 = \sum_{i=1}^{N_m} \sqrt{\frac{1}{N} \sum_{j=1}^{N} (m^i_{\text{true}} - m^i_j)^2}, \tag{9}$$

where $N$ is the ensemble size, $N_m$ is the number of grid blocks, $m^i_{\text{true}}$ is the value at node $i$ in the reference field, and $m^i_j$ is the value at node $i$ in the $j$th facies indicator realization of the ensemble.

## 6. Results and Discussion

### 6.1. Evolution of the Data Mismatch

The proposed conditioning approach was first tested by assimilating the transient hydraulic head data generated from the Reference "A" (Figure 10) at the 10 observation points (Figure 8). Based on 6 × 41 hard conditioning points located approximately every two cells in the vertical direction and every three cells horizontally, hence a sampling rate of 15% at the coarsest level, a convergence of the reduction of the head data mismatch was observed (Figure 14). Figure 15 confirms that the data match at every head observation point was effectively improved after 16 ES-MDA iterations. In addition, the flow rate observations were well predicted by the final categorical fields although they were not considered for the assimilation.

As explained in section 2, the same seed value and same hard conditioning locations for all ensemble members during the conditioning loop ensure that the convergence can be fully attributed to the integration of the ES-MDA update at those points. We also repeated the test using other unique seed values than the one indicated in Table 1 and observed each time a convergence of the approach.

In comparison to applications of ensemble Kalman methods in the multi-Gaussian case or in MPS cases without facies resimulation within the update procedure, it is worth mentioning that the decrease of the

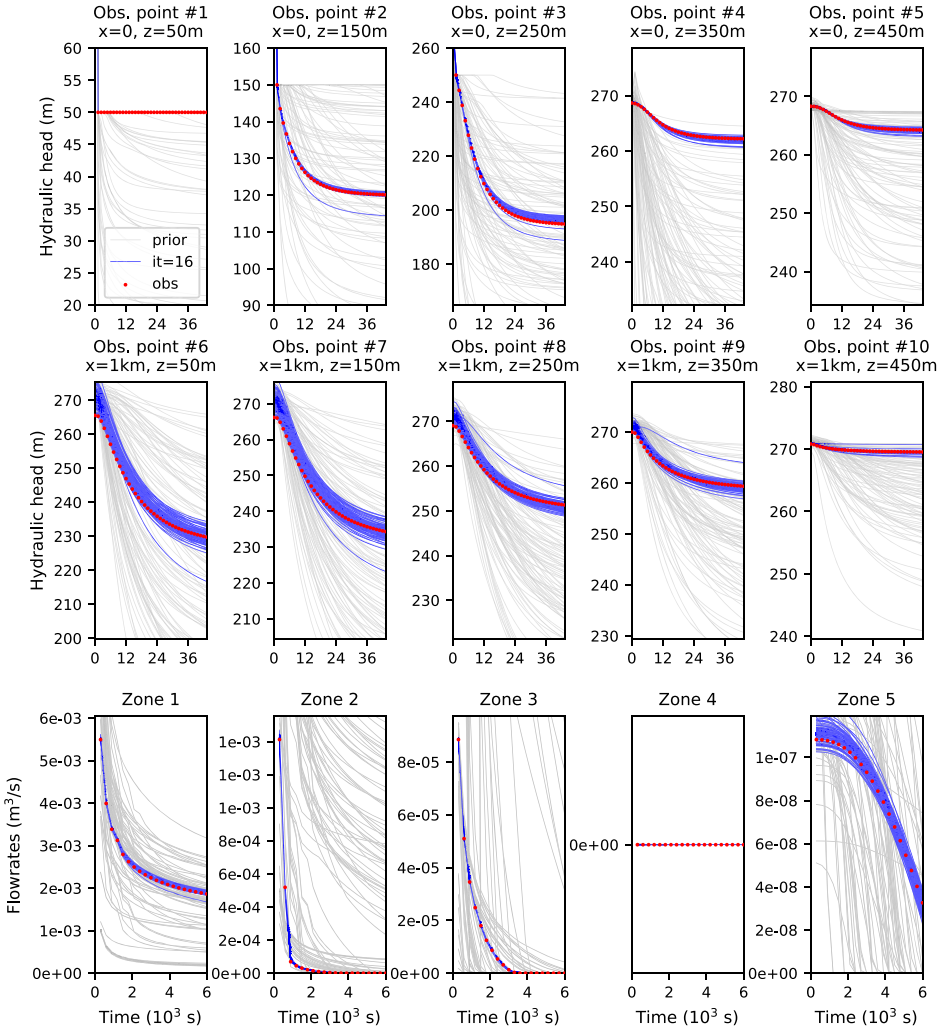


**Figure 15.** Predicted hydraulic head and flow rate data at the observation locations, before (in gray) and after (in blue) the assimilation of the hydraulic heads only. The red dots are the observed data; the ensemble size is 100.

data mismatch observed here is not as smooth. Similarly to the updating of truncated Gaussian realizations via the underlying multi-Gaussian variables, the oscillations during the reduction of the mismatch are indicative of nonlinearities in the forward operator relating the parameter variables and the dynamic data to assimilate. In this categorical MPS case by using the proposed approach, the oscillations can be large because the process allowing to obtain the categorical field from the coarsest-scale parameters; that is, the multiresolution MPS simulation is nonlinear in the same manner as the truncation step is nonlinear in the truncated Gaussian case (Liu and Oliver, 2005).

### 6.2. Sensitivity to DeeSse Parameters of the Integration of the ES-MDA Update

As shown in Table 1, we allowed in the tests to further scan the TI at both coarse levels including the one where the ES-MDA update is integrated. In the context of the proposed methodology, the maximal scanned fraction at the coarse scales can indeed influence the convergence of the algorithm. It makes sense since by increasing the scanned fraction of the coarsest TI, the more likely a more compatible pattern, which include the hard data derived from the ES-MDA update will be found, and hence the better the integration of the ES-MDA update will be. It is worth noting that this constraint on the maximal scanned fraction at the coarse levels should be computationally affordable. Indeed, given the significant reduction by a factor 4 of the simulation grid at each coarse level, the search for patterns in the corresponding TI will also be faster.

By testing several distance thresholds, we observed that a value lower than 0.01 or greater than 0.1 would result in a less efficient convergence and an insufficient data match. Even if the history match had turned

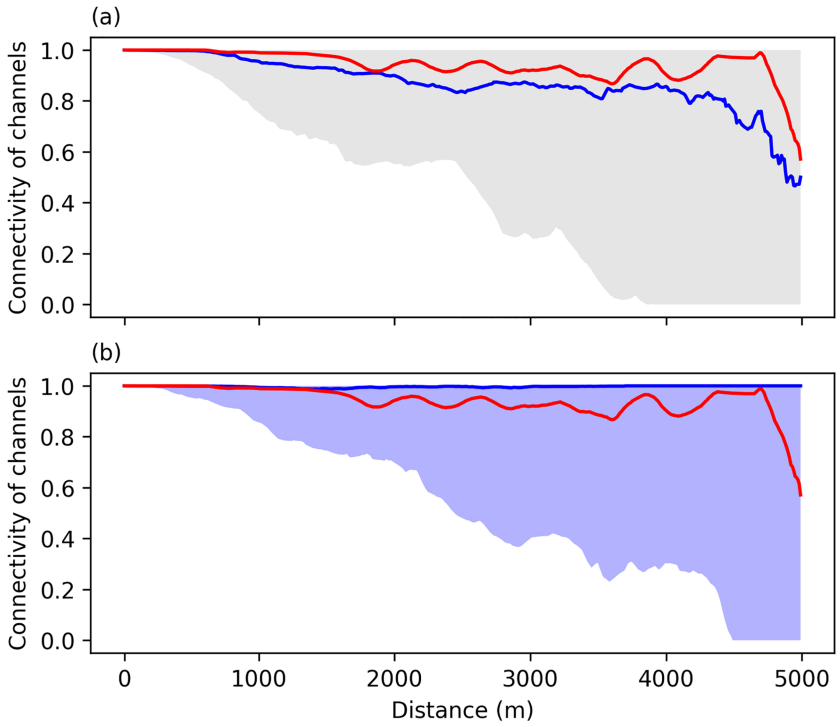


**Figure 16.** Connectivity function of the channel facies computed for the ensemble of categorical MPS simulations: (a) before the update (b) after all the ES-MDA updates. The gray and blue regions correspond to the values between the Percentiles P5 and P95. The red curve is the connectivity function calculated with Reference A and the blue curve is the median of the ensembles of values taken by the connectivity function.

out to be acceptable, the biggest issue was the fact that these tested values did not allow the retrieval of the expected structures after the data assimilation. After some tuning, we found that a value around 0.05 was a good compromise to obtain simultaneously both a good history match and plausible structures. The consistency of the retrieved structures is confirmed by evaluating the connectivity function of the channel facies for each final categorical MPS realization. Figure 16 shows that the range of final connectivity values obtained is consistent with the range obtained with the initial facies fields generated before the conditioning. The median values before and after the assimilation indicate a global increase of the connectivity of the channel facies.

It is important to keep in mind that in the proposed approach, the hard conditioning points used at the coarsest scale of the multiscale MPS simulations do not represent actual data but are only the result of the back transformed parameters updated with ES-MDA at those points. Since ES-MDA updates the parameters iteratively and in doing so improves the estimates over the iterations, it also means that the values at the sampled hard conditioning points will correspond to less good estimates at the first iterations of ES-MDA. This is especially true in a non-multi-Gaussian case with the degradation of the structures as soon as the first ES-MDA update is applied. As a result, in order for our conditioning approach to be successful, DeeSse must take on the critical role of helping retrieve the structures especially during the early iterations of ES-MDA by not giving too much weight to the first estimates of the hard conditioning points. That is why defining a too low distance threshold value, such as 0.01, does not make sense here because DeeSse should not too rigorously search for matching patterns given the inaccurate first ES-MDA estimates as hard data. Instead, the threshold should be defined in order to allow some flexibility when accommodating the less reliable estimates of the first iterations. In this way, DeeSse will give preference to the simulation of patterns that are as consistent as possible to the TI given the hard conditioning points, rather than try to exactly honor them at the beginning of the data assimilation and simulate inconsistent structures. However, if this distance threshold is too large, for example, 0.1, the ES-MDA updates at the later iterations will be on the contrary not sufficiently integrated into the multiresolution MPS simulations, thereby compromising the efficient convergence of the conditioning approach. Even though it was not tested, one may consider to adapt the

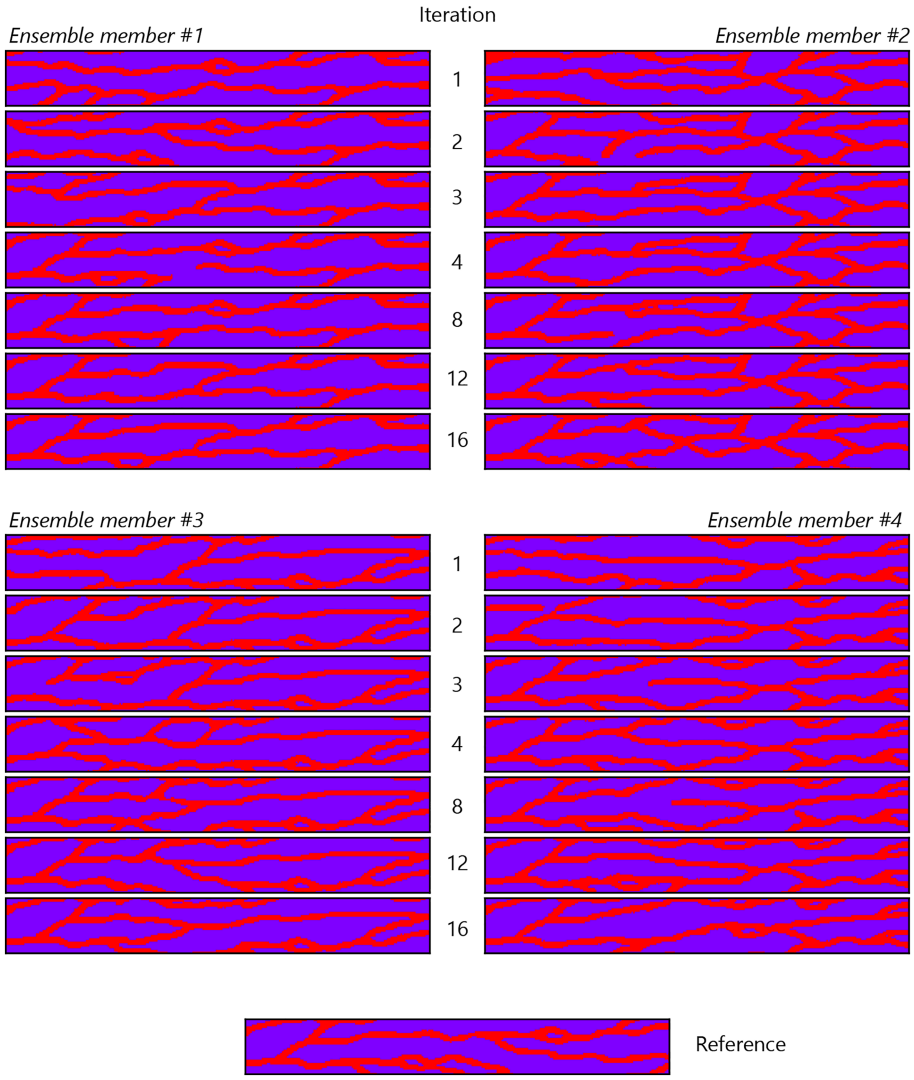


**Figure 17.** Conditioned categorical MPS simulations obtained after certain iterations of ES-MDA out of 16 in total, for four ensemble members. The image at the bottom is the Reference Field A.

threshold in a decreasing manner from one iteration to another to improve the integration of the update and hence the robustness of the convergence.

### 6.3. Identification of the Categorical Fields

Figure 17 shows the categorical realizations obtained at different stages of the conditioning procedure for four ensemble members. As expected, the simulated structures become more and more consistent over the ES-MDA iterations. Although not shown here for brevity, the $RMSE_2$ calculated in the updated region has decreased, thereby confirming that the conditioned fields resemble the reference. The probability maps of the channel facies, calculated before and during the conditioning (Figure 18), shows the progressive identification of the structures and retrieval of the connectivity during the assimilation. In between the two columns of observation points, the channels are characterized with a very low uncertainty and they look very much like the channels of the Reference A in the same region. Upstream to the last locations informed by data, at around $x = 2,500$ m, a progressive increase of uncertainty can also be observed. Overall, the identification of the parameters is consistent with the distribution of the data points and the distance-based localization that was applied to restrain the update to the vicinity of the data points.

As shown in Figure 19, the ensemble spread calculated from the facies realizations significantly decreased in the updated region during the data assimilation. In our case, this ensemble spread represents on average, in the updated region, the spread around the probability of the channel facies.

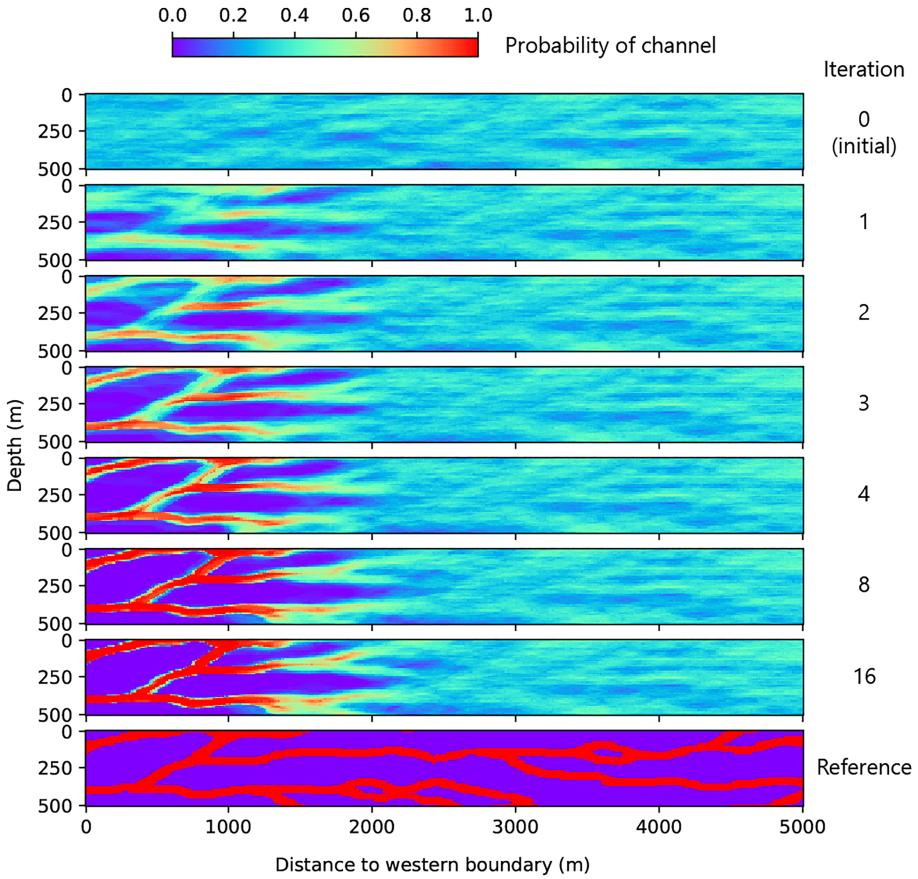


**Figure 18.** Probability map for the channelized facies calculated from the ensemble of categorical MPS simulations before conditioning and after every two iterations of ES-MDA using the hydraulic head observations from Reference A (shown at the bottom).

In the non-multi-Gaussian bimodal case of log hydraulic conductivity fields, Zhou et al. (2011) illustrated the influence of the ensemble size on the accuracy of the estimated uncertainty with the NS-EnKF approach. They concluded that using an ensemble size of the order of 100, such as in our example, led to a severe uncertainty underestimation as quantified by the very large discrepancy between the ensemble spread and the RMSE at the end of the data assimilation.

While the RMSE is an appropriate measure of the true uncertainty in the multi-Gaussian case, we note that it is not a rigorous one in the discrete case. In the multi-Gaussian case, it is assumed that the reference field is the mean of a multi-Gaussian distribution of realizations, which are all conditioned to the data. It therefore makes sense to calculate in that case the distance between the ensemble mean and the reference in order to obtain an estimation of the true error. In the discrete case, however, the reference field is a random sample from a distribution, which can be much more complex. Hence, the RMSE that measures the distance between this reference sample and the ensemble mean could ultimately result in a large underestimation of the true uncertainty. Therefore, although it can be observed in Figure 19 that both the ensemble spread and RMSE decrease to a same value after all the updates thanks to the proposed methodology, this convergence ultimately does not tell us how accurate the estimated uncertainty is.

To test the uncertainty estimated with our approach, we used the rejection sampling method to generate samples from the posterior distribution and used it as the reference distribution. Rejection sampling consists in sampling from the prior distribution of unconditional categorical realizations and accepting each sample with a probability calculated based on the ratio between the likelihood of the sample and the highest likelihood value, which can be obtained (Tarantola, 2005). The ensemble of accepted samples follows the posterior distribution. Figure 20a shows the probability map obtained based on 108 samples, which have been accepted out of 185,000 unconditional realizations generated with DeeSse. By visually comparing this

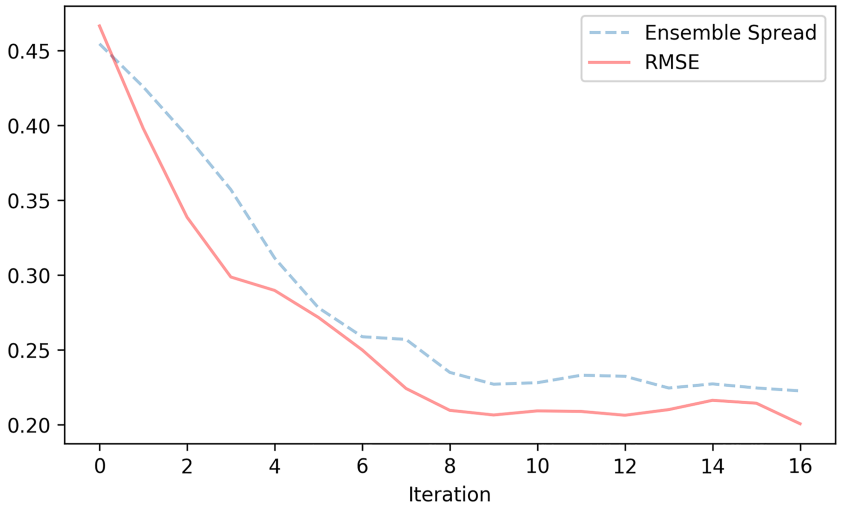


**Figure 19.** Evolution of the RMSE and the ensemble spread (both unitless) before and during the conditioning of the categorical MPS realizations in the updated region (up to 1,600 m from the seepage boundary) for the ES-MDA update with the synthetic data of Reference A.

map to the one calculated based on the ensemble of 100 conditioned categorical fields obtained by data assimilation using our proposed methodology (Figure 20b), we can see clearly that the posterior distribution obtained by rejection sampling also identifies with very low uncertainty the location of the channels in the same region, which was updated by data assimilation using our proposed approach, that is, up to $x = 1,600$ m from the western boundary. Moreover, the structures identified by both approaches in this region are very similar to each other. To measure quantitatively how one distribution is different from another distribution, one could, for example, calculate the Kullback-Leibler divergence (Kullback & Leibler, 1951). For this case, a low value close to 0 was calculated and indicates that the two distributions are indeed very similar. Therefore, we can finally conclude that the uncertainty reduction, which led to the identification of the categorical fields with very low uncertainty using our proposed methodology is mostly the result of an efficient assimilation of the data rather than to a suboptimal application of the ensemble Kalman method due to an insufficient ensemble size as pointed out for example in Zhou et al. (2011) or Chen and Zhang (2006).

Despite the use here of a small ensemble size of 100, we assume that the efficiency of the proposed data assimilation methodology results from the combined effect of (1) the reduction of the number of parameters via the multiresolution parameterization and the sampling and (2) the role of DeeSse in finding consistent patterns. Indeed, although the whole coarsest-resolution field was updated in our case, the number of effective parameters was ultimately the number of sampled hard conditioning points, hence 246. Given the

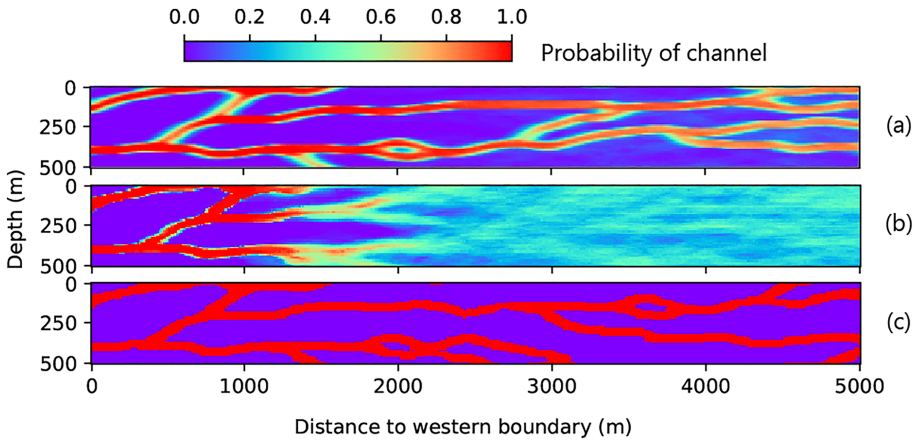


**Figure 20.** (a) Probability map obtained by rejection sampling. (b) Probability map obtained after the final update at iteration 16 with the proposed methodology. (c) Reference field.

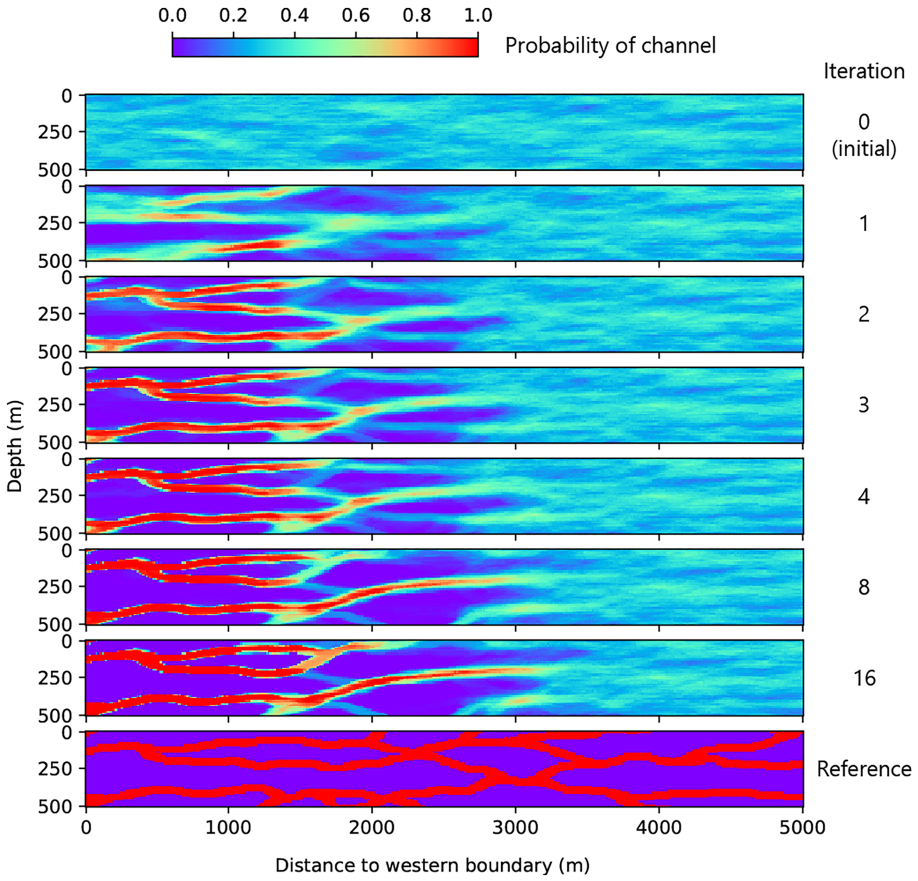


**Figure 21.** Probability map for the channelized facies calculated from the ensemble of categorical MPS simulations before conditioning and after every two iterations of ES-MDA using the hydraulic head observations from Reference B (shown at the bottom).

ensemble size of 100, we can assume that the covariance matrices were more correctly approximated from the ensemble.

### 6.4. Analysis of Case B

To further assess the performance of the proposed methodology, we also performed tests using the synthetic set of head data generated from the Reference Field B (Figure 11). A longer critical length of 2,600 m was defined in this case to take into account the larger extent of the drawdown at the last time step of the synthetic data set (Figure 13). Therefore, the region of parameters to update by data assimilation in this case was also larger.

Using a similar density of sampled hard conditioning points as in the previous case with Reference A, the approach converged successfully and towards a good final match of the transient head and flow rate data. (We do not illustrate those results here for the sake of brevity.) However, we note from Figure 21 that upstream from the second set of data points, between approximately $x = 1,600$ m and $x = 2,600$ m, the very low uncertainty on the updated channel locations is clearly inaccurate given how very few channels were identified and how the channels seem less connected compared to our prior knowledge from the TI. We can therefore conclude that the uncertainty in this area, which is less informed by data, is significantly underestimated. Figure 22 shows a much larger reduction of the ensemble spread compared to the RMSE in the updated region up to 2,600 m from the seepage boundary, confirming that those very low probabilities of channels between 1,600 and 2,600 m after the data assimilation in Figure 21 should not be relied upon.

Although we do not show it here for brevity, the RMSE actually decreases in the same manner as the ensemble spread if only the region up to 1,600 m from the seepage boundary is considered. This indicates that the uncertainty is better estimated in this more informed area of the updated region. Also, the decrease of the RMSE suggests that the data assimilation was especially efficient with probabilities of channels getting

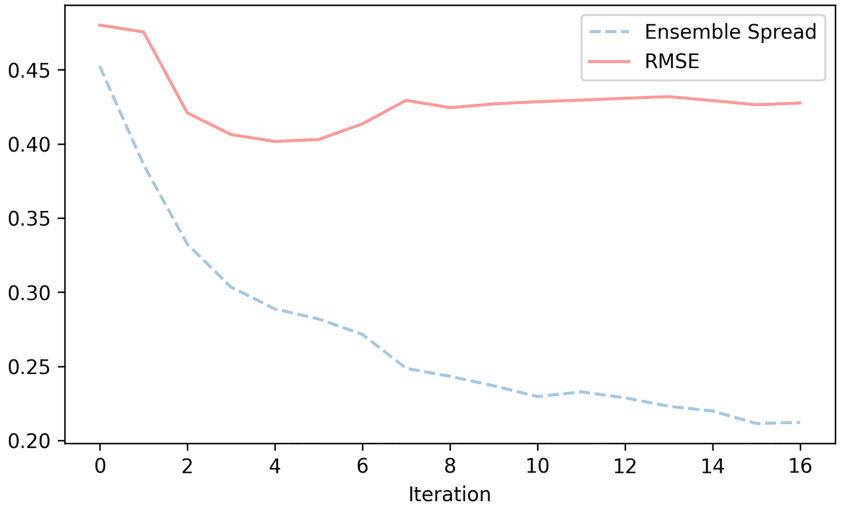


**Figure 22.** Evolution of the RMSE and the ensemble spread (both unitless) before and during the conditioning of the categorical MPS realizations in the updated region (up to 2,600 m from the seepage boundary) for the ES-MDA update with the synthetic data of Reference B.

closer to the reference which represents here the indicator values of the channel facies. Figure 21 shows clearly the much more consistent structures before $x = 1,600$ m and also that the identified structures look very much like those from the reference in the same region.

Considering that the number of parameters to update in this Case B is larger than in the previous Case A, we assume that the severe underestimation of the uncertainty observed beyond $x = 1,600$ m in the update region is related to spurious correlations affecting the computed parameter updates. Indeed, the observation points at $x = 0$ m and $x = 1,000$ m may be too distant from the parameters located in that region to inform them with sufficient accuracy by ensemble data assimilation. As mentioned in section 3.2, the performance of ensemble Kalman methods can be severely reduced by an excessive underestimation of the uncertainty due to spurious correlations between parameters and observations far apart.

To avoid those inaccurate estimations and resulting inconsistencies in the conditional categorical fields, a solution could be to sample the predefined hard conditioning points only at locations of the updated region which are sufficiently informed by nearby observations. In this manner, locations that are likely to be affected by spurious correlations can be simulated with DeeSse instead, thereby preventing the unreliable updates from being taken into account in the multiresolution MPS simulation. Although this strategy is ad hoc, it is somewhat very similar to the way the widely used and also ad hoc covariance inflation method must be implemented in practice. As pointed out by Hamill and Whitaker (2005), inflating the ensemble spread uniformly over the whole model domain will lead to an undesirable unbounded growth of the ensemble variance at locations with nearly nonexistent data. Hence, while covariance inflation should be performed only in areas experiencing a significant uncertainty reduction, that is, near the observation locations, the sampling of the updated conditioning points in our proposed methodology should be performed similarly only near the observation locations since those sampled points will not be affected too negatively by the unavoidable long range spurious correlations. Figure 23 illustrates this sampling strategy close to the observations located at $x = 0$ m and $x = 1,000$ m, hence leaving out the uninformed part between $x = 1,600$ m and $x = 2,600$ m of the updated region.

As can be observed in Figure 23, it is important for the stability of the results to also have hard conditioning points sampled from the nonupdated region, that is, beyond $x = 2,600$ m. Indeed, those invariant samples will ensure that the simulated structures do not noticeably change from one iteration to the other in this area, thereby allowing approximately the same contribution from this region to affect the predicted flow observations. We assume that such invariant contribution throughout the iterations affect positively the related covariance matrices by making the parameter estimation more tractable for the proposed methodology. As suggested by the probability maps obtained using this adaptive sampling strategy (Figure 24), the consistency of the identified structures is this time preserved during the data assimilation no matter the locations

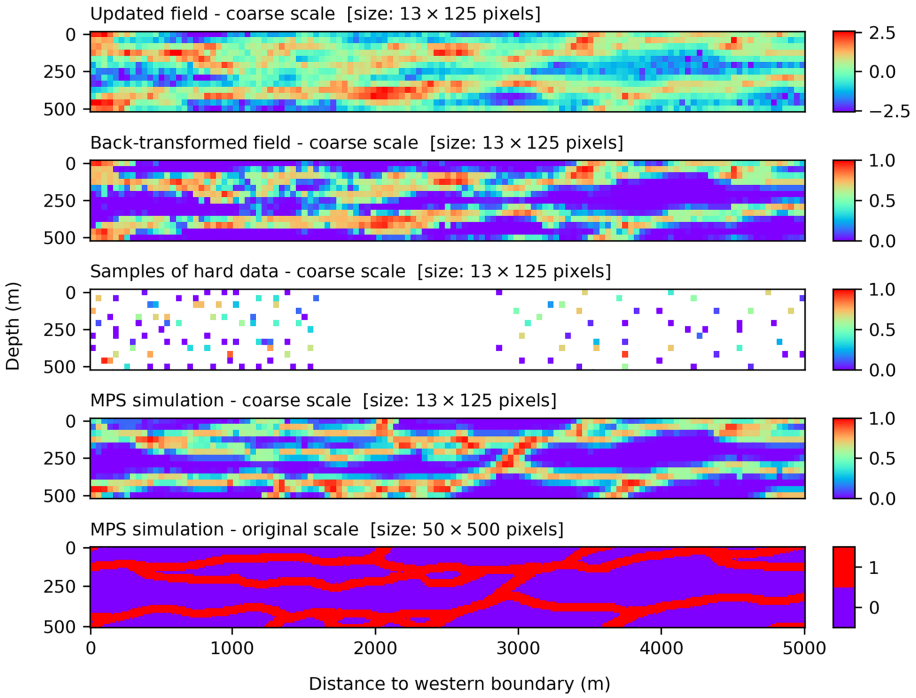


**Figure 23.** Conditioning a categorical MPS realization (bottom image) from the updated normal-scored image at the coarsest pyramid scale (Ensemble Member No. 11) at iteration 8 out of 16 of ES-MDA (top image) via fixed conditioning points sampled from the back-transformed image near the observation observations for the multiresolution MPS simulation.

of the observations in the updated region. Moreover, despite the larger role given to DeeSse here in the uninformed regions, the proposed methodology still converged successfully towards a good final match of the transient head and flow rate data (Figure 25).

Ultimately, the Case B illustrates the broader applicability of the proposed methodology in more realistic situations where the observation points may not be evenly distributed in the region of interest for the parameter identification.

### 6.5. Comparison With Other Approaches

We consider that the greatest advantage of the proposed methodology is the nature of the link between the continuous latent variables updated by the ensemble Kalman method and the conditioned facies fields. The Gaussian pyramid technique relates directly the value of the latent variable at a coarse resolution with the categorical patterns for a given realization at a finer scale. It allows a reduction of the dimension of the problem and gives a direct relation between the continuous values and the facies field.

Among the previously published methods, a classical technique is to use the local hydraulic properties as a latent variable and avoid using the facies during the update. For example, the NS EnKF (Zhou et al., 2011) updates the continuous hydraulic conductivities populating an initial ensemble of facies distribution in a full postprocessing procedure. We note that for such approach to work, the hydraulic conductivities must be defined in a continuous manner otherwise the NS transform function will not be defined. In the proposed approach, although the exact same NS transform is used, the advantage is that the latent variable is by construction necessarily continuous at every location of the coarsest resolution level (Figure 4).

Cao et al. (2018) proposed to update only the conductivity values at randomly selected pilot points. The updated values are then used as hard data for a conditional MPS simulation with a TI representing continuous log hydraulic conductivities that populate a categorical facies field. Their motivation for using pilot points was actually the same as ours. Indeed, they noticed that updating the whole field of log hydraulic conductivities with iterative ensemble smoothing do not allow to preserve the prior non-Gaussian spatial patterns. Following the same strategy, we do not update the complete coarsest resolution. But unlike Cao et al. (2018) who apply the updates at the fine resolution, our approach will better preserve the structures

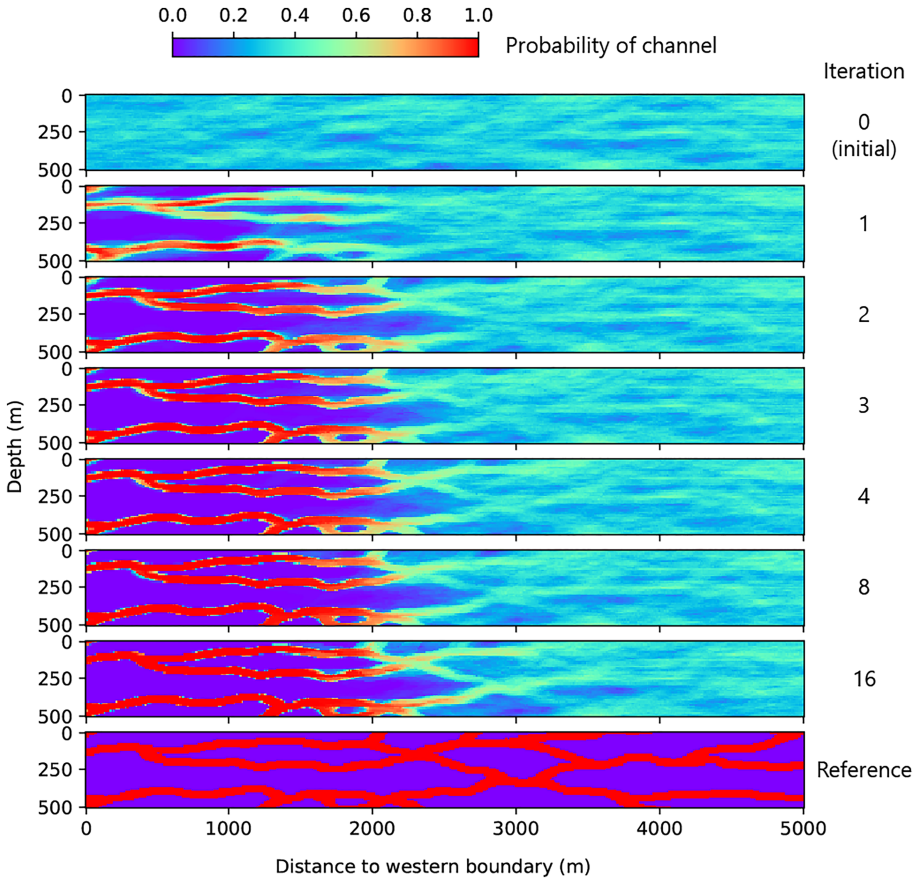


**Figure 24.** Probability map for the channelized facies calculated from the ensemble of categorical MPS simulations before conditioning and after every two iterations of ES-MDA using the hydraulic head data generated from Reference B (bottom image). The hard conditioning point locations as shown in Figure 23 were used.

even if the updates are applied on the complete field at the coarsest scale because of the multiresolution strategy.

Still considering the use of hydraulic conductivities as primary variables for the EnKF update is possible when the TI is continuous as used for example in Cao et al. (2018). Although it is beyond the scope of this study, it is worth mentioning that multiresolution simulations with DeeSse based on a continuous TI originally can also be performed. Therefore, the proposed methodology is not limited to the categorical case described in the synthetic example treated in this paper but could also be applied in the continuous case. As compared to previous work, the gain would again be the reduction of problem dimensions through the use of the pyramids.

Ultimately, comparing the NS-EnKF to our approach, we note that the reduction of the data mismatch seems to be more efficient for all members of the final ensemble with our proposed method. This could be attributed to the randomness of the conditional MPS simulations, which is probably not sufficiently constrained as in our proposed methodology with both the use of the same seed and the same fixed hard conditioning points for all ensemble members. Another reason for the mismatch could be related to the fact that no other mitigation strategies than the pilot points are employed to reduce the loss of consistency of the simulated structures. Indeed, we believe that the multiresolution parameterization alone in our approach allows to alleviate this problem and will ultimately positively influence the correction applied at the hard conditioning points.

Another interesting approach is the probability conditioning method of Jafarpour and Khodabakhshi (2011). It also uses the hydraulic conductivity as a continuous variable to update the fields, but here the link with the categorical MPS simulations is controlled using a probability map. The updated variables are related to the facies distribution in an indirect manner. At each iteration, the hydraulic conductivities are updated, and a

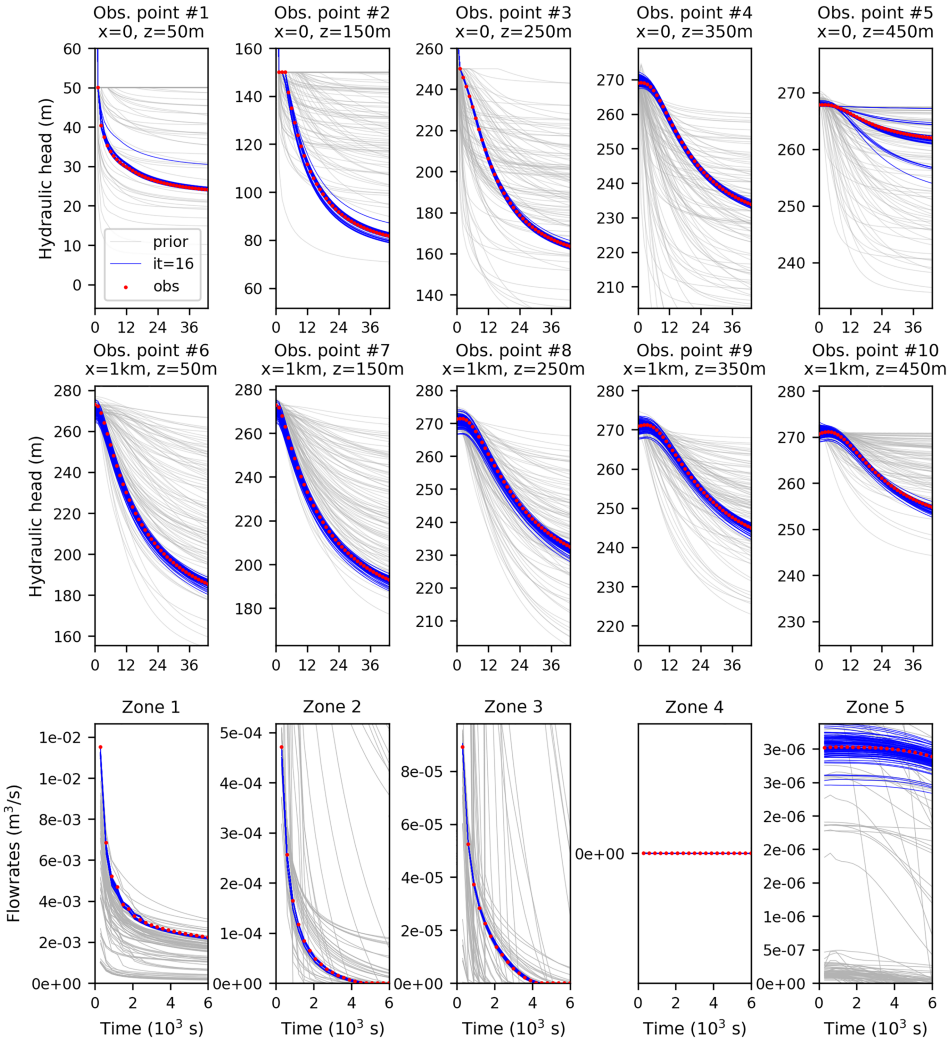


**Figure 25.** Predicted hydraulic head and flow rate data at the observation locations, before (in gray) and after (in blue) the assimilation of the hydraulic heads only. The red dots are the observed data; the ensemble size is 100. The hard conditioning point locations as shown in Figure 23 were used.

probability map is derived from the mean of the ensemble of updated log hydraulic conductivity field using some assumed triangular probability density functions. Once the corrected probability map is obtained, a new set of MPS simulations is generated. All these simulations are conditioned to this unique probability map using SNESIM and the $\tau$ model. Although this step allows to control the conditional facies MPS realizations, the derived probability maps are prone to significant noise due to the initial non-multi-Gaussian distribution of hydraulic conductivities, and the structures are not well preserved.

Ma and Jafarpour (2018) proposed recently a pilot point parameterization for the hard conditioning of categorical MPS simulations with an ensemble Kalman approach. Similarly to Cao et al. (2018), an ensemble of log hydraulic conductivities is updated without prior NS transform. Also, in the same manner as in the probability conditioning method, the values estimated at the pilot points are converted to facies probabilities. These probabilities are then used to sample a facies type, thereby allowing a conditioned categorical MPS simulation using the updated facies as hard data. However, unlike Cao et al. (2018) or in our proposed approach, they select the hard conditioning points based on the combined information of the sensitivity of the model response to the parameters and the variance of the parameters based on the ensemble of log hydraulic conductivity fields. As a result, one main difference with our approach is that when using ES-MDA, the locations of the pilot points may change from one iteration to another according to the updated sensitivity and parameter variance. As observed by the less efficient reduction of the data mismatch com-

pared to our proposed methodology, the randomness introduced by each conditional MPS simulation with the proposed selection of pilot points may lead to a less tractable and hence less robust convergence.

Finally, as illustrated in our case with the Reference A, provided that the ES-MDA update is applied with care to avoid underestimating the uncertainty in insufficiently informed areas, it is conceptually simpler to rely on ES-MDA to compute proper estimates of the parameter and variance no matter the location. In this way, we can consider that every location can potentially be a hard conditioning point. Then, the choice of only a subset of locations can be done in a simple, uniform manner enabling DeeSse to properly retrieve the structures inferred by ES-MDA in between the same fixed locations and by using the same seed for all ensemble members.

As an alternative to the standard EnKF, Zhou et al. (2012) also proposed the Ensemble PATtern matching method which was then further applied and extended (Li et al., 2014; Lochbühler et al., 2014). Unlike the proposed methodology, which still relies on the linear update step of ensemble Kalman methods, the update step in Ensemble PATtern is fully replaced by the search of matching conditional patterns composed of both model parameters and state observations. Although this method ensures by construction the reproduction of curvilinear patterns at multiple scales, a main drawback, however, is the very large number of realizations required for the matches to be found (Li et al., 2014).

## 7. Conclusions

In this paper, a new approach to condition categorical MPS realizations with an iterative ensemble Kalman method was introduced. The methodology uses a multiresolution parameterization with the code DeeSse based on the Gaussian pyramid technique, which massively reduces the number of parameters to update. Initially, these parameters correspond to the NS transformed values of the coarsest level of a multiresolution MPS simulation. After each update, the parameters can be integrated at the coarsest level of a multiresolution MPS simulation to finally condition the categorical simulation performed at the scale of the original categorical TI. Although it was not in the scope of this study, it is worth pointing out the applicability of the same multiresolution parameterization to originally continuous cases as well.

At the coarsest scale of the multiresolution MPS simulation, only a subset of locations are updated with ES-MDA. As a result, the methodology also heavily relies on the ability of DeeSse to recover the structures by the integration, as hard data, of the result of each data assimilation. The more the number of hard conditioning points considered, the more control over the data match, but the less control over the consistency of the simulated structures. However, our results obtained for two synthetic examples show that the proposed multiresolution parameterization has the potential to satisfy simultaneously both the requirements on the quality of the data match and the consistency of the updated fields with the prior geological information. Because the locations of the hard conditioning points are chosen to be fixed, and identical for all ensemble members throughout the assimilation, our specified parameterization of the ensemble of multiresolution MPS simulations effectively ensures the stability of the proposed algorithm. Indeed, the robust convergence observed in our synthetic case, for any of the two tested references, can unambiguously be attributed to the improved estimated values at the hard conditioning points throughout the assimilation.

Our numerical experiments tend to show that both the multiresolution framework and the sampled hard conditioning points contribute to mitigate the limitations resulting from the ensemble Kalman method in our non-multi-Gaussian case. As long as the amount of information given by the synthetic data is sufficient to identify the region of interest, our results show that the proposed methodology can successfully condition facies realizations that both honor the dynamic observations and are consistent with the prior conceptual model.

Moreover, the important uncertainty reduction during the conditioning procedure has been shown to be the consequence of a particularly efficient parameter identification, rather than an underestimation related to a suboptimal application of the ensemble Kalman method. We can assume that the improved performance of the ensemble Kalman method is mainly related to the massive parameter reduction, which ultimately allowed to reduce the discrepancy with the limited ensemble size used and hence to obtain more accurate updates. In addition, DeeSse plays an undeniable role in the significant observed decrease of the RMSE considering that its goal, ultimately, is to find compatible patterns in a TI that was used to simulate the

reference fields of this synthetic case. The use of a unique TI to generate both the reference and the MPS simulations involved during the conditioning procedure is indeed a simplification made to evaluate the proposed approach in the situation where the conceptual geological model is consistent with the reality. For real cases, different TIs should be tested during the conditioning procedure.

In conclusion, although the results presented in this paper illustrate the performance of our methodology in a synthetic case with only two simulated facies, the same methodology can be applied to any number of simulated facies. The pyramid of TIs has indeed been shown to work in the multicategorical case (Straubhaar et al., 2020). The ensemble Kalman method would then be applied to update the values of not only one initial coarse MPS simulation generated for each ensemble member but several initial coarse MPS simulations generated from each facies indicator field. Since the number of grid blocks at the coarsest level is significantly reduced, and because only a subset of locations will be considered for the update ultimately, the increased number of parameters when considering a large number of facies could in practice still be much lower than the number of unknown in the categorical simulation.

**Acknowledgments**
The authors would like to thank the Faculty of Science (University of Neuchâtel) for providing the computational resources that allowed to achieve this work. They also thank Pierre Perrochet (Université de Neuchâtel) and Hakim Benabderrahmane (ANDRA) for the information regarding the real situation that inspired the synthetic case presented in this paper. A package with the data used in this paper can be found on GitHub (https://github.com/randlab/agate).

## References

Abadpour A., Adejare M., Chugunova T., Mathieu H. & Haller N. (2018), Integrated geo-modeling and ensemble history matching of complex fractured carbonate and deep offshore turbidite fields, generation of several geologically coherent solutions using ensemble methods, Society of Petroleum Engineers (SPE), doi:https://doi.org/10.2118/193028-ms.

Anderson, J. L. (2012). Localization and sampling error correction in ensemble kalman filter data assimilation. *Monthly Weather Review*, *140*(7), 2359–2371. https://doi.org/10.1175/mwr-d-11-00013.1

Benabderrahmane, H., Kerrou, J., Tacher, L., Deman, G., & Perrochet, P. (2014). Modelling of predictive hydraulic impacts of a potential radioactive waste geological repository on the Meuse/Haute-Marne multilayered aquifer system (France). *Journal of Applied Mathematics and Physics*, *02*(12), 1085–1090. https://doi.org/10.4236/jamp.2014.212125

Burt, P., & Adelson, E. (1983). The laplacian pyramid as a compact image code. *IEEE Transactions on Communications*, *31*(4), 532–540. https://doi.org/10.1109/TCOM.1983.1095851

Cao, Z., Li, L., & Chen, K. (2018). Bridging iterative ensemble smoother and multiple-point geostatistics for better flow and transport modeling. *Journal of Hydrology*, *565*(May), 411–421. https://doi.org/10.1016/j.jhydrol.2018.08.023

Chen, Y., & Zhang, D. (2006). Data assimilation for transient flow in geologic formations via ensemble Kalman filter. *Advances in Water Resources*, *29*(8), 1107–1122. https://doi.org/10.1016/j.advwatres.2005.09.007

Cornaton F. (2014), Ground Water (GW) A 3-D ground water and surface water flow, mass transport and heat transfer finite element simulator, Tech. rep., University of Neuchâtel.

Deman, G., Konakli, K., Sudret, B., Kerrou, J., Perrochet, P., & Benabderrahmane, H. (2015). Using sparse polynomial chaos expansions for the global sensitivity analysis of groundwater lifetime expectancy in a multi-layered hydrogeological model. *Reliability Engineering and System Safety*, 147, 156–169. https://doi.org/10.1016/j.ress.2015.11.005

Emerick, A. A. (2016). Analysis of the performance of ensemble-based assimilation of production and seismic data. *Journal of Petroleum Science and Engineering*, *139*, 219–239. https://doi.org/10.1016/j.petrol.2016.01.029

Emerick, A. A., & Reynolds, A. C. (2012). Ensemble smoother with multiple data assimilation. *Computers and Geosciences*, *55*, 3–15. https://doi.org/10.1016/j.cageo.2012.03.011

Evensen, G. (1994). Sequential data assimilation with a nonlinear quasi-geostrophic model using Monte Carlo methods to forecast error statistics. *Journal of Geophysical Research*, *99*(C5), 10,143–10,162. https://doi.org/10.1029/94jc00572

Evensen, G. (2009). The ensemble Kalman filter for combined state and parameter estimation: Monte Carlo techniques for data assimilation in large systems. *IEEE Control Systems*, *29*(3), 83–104. https://doi.org/10.1109/MCS.2009.932223

Evensen, G. (2018). Analysis of iterative ensemble smoothers for solving inverse problems. *Computational Geosciences*, *22*(3), 885–908. https://doi.org/10.1007/s10596-018-9731-y

Gardet, C., Le Ravalec, M., & Gloaguen, E. (2014). Multiscale parameterization of petrophysical properties for efficient history-matching. *Mathematical Geosciences*, *46*(3), 315–336. https://doi.org/10.1007/s11004-013-9480-3

Gaspari, G., & Cohn, S. E. (1999). Construction of correlation functions in two and three dimensions. *Quarterly Journal of the Royal Meteorological Society*, *125*(554), 723–757. https://doi.org/10.1256/smsqj.55416

Hamill, T. M., & Whitaker, J. S. (2005). Accounting for the error due to unresolved scales in ensemble data assimilation: A comparison of different approaches. *Monthly Weather Review*, *133*(11), 3132. https://doi.org/10.1175/MWR3020.1

Heidari, L., Gervais, V., Ravalec, M. L., & Wackernagel, H. (2013). History matching of petroleum reservoir models by the ensemble Kalman filter and parameterization methods. *Computers and Geosciences*, *55*, 84–95. https://doi.org/10.1016/j.cageo.2012.06.006

Houtekamer, P. L., & Mitchell, H. L. (2006). Ensemble Kalman filtering. *Quarterly Journal of the Royal Meteorological Society*, *131*(613), 3269–3289. https://doi.org/10.1256/qj.05.135

Hu, L. Y., Zhao, Y., Liu, Y., Scheepens, C., & Bouchard, A. (2013). Updating multipoint simulations using the ensemble Kalman filter. *Computers and Geosciences*, *51*, 7–15. https://doi.org/10.1016/j.cageo.2012.08.020

Jafarpour, B., & Khodabakhshi, M. (2011). A probability conditioning method (PCM) for nonlinear flow data integration into multipoint statistical facies simulation. *Mathematical Geosciences*, *43*(2), 133–164. https://doi.org/10.1007/s11004-011-9316-y

Kerrou, J., Deman, G., Tacher, L., Benabderrahmane, H., & Perrochet, P. (2017). Numerical and polynomial modelling to assess environmental and hydraulic impacts of the future geological radwaste repository in Meuse site (France). *Environmental Modelling and Software*, *97*, 157–170. https://doi.org/10.1016/j.envsoft.2017.07.018

Kullback, S., & Leibler, R. A. (1951). On information and sufficiency. *The Annals of Mathematical Statistics*, *22*(1), 79–86.

Li, L., Srinivasan, S., Zhou, H., & Gómez-Hernández, J. J. (2014). Simultaneous estimation of geologic and reservoir state variables within an ensemble-based multiple-point statistic framework. *Mathematical Geosciences*, *46*(5), 597–623. https://doi.org/10.1007/s11004-013-9504-z

Li, L., Zhou, H., Hendricks Franssen, H. J., & Gómez-Hernández, J. J. (2012). Groundwater flow inverse modeling in non-MultiGaussian media: Performance assessment of the normal-score ensemble Kalman filter. *Hydrology and Earth System Sciences*, *16*(2), 573–590. https://doi.org/10.5194/hess-16-573-2012

Liu, N., & Oliver, D. S. (2005). Ensemble Kalman filter for automatic history matching of geologic facies. *Journal of Petroleum Science and Engineering*, *47*(3-4), 147–161. https://doi.org/10.1016/j.petrol.2005.03.006

Lochbühler, T., Pirot, G., Straubhaar, J., & Linde, N. (2014). Conditioning of multiple-point statistics facies simulations to tomographic images. *Mathematical Geosciences*, *46*(5), 625–645. https://doi.org/10.1007/s11004-013-9484-z

Ma, W., & Jafarpour, B. (2018). Pilot points method for conditioning multiple-point statistical facies simulation on flow data. *Advances in Water Resources*, *115*, 219–233. https://doi.org/10.1016/j.advwatres.2018.01.021

Ma, W., & Jafarpour, B. (2019). Integration of soft data into multiple-point statistical simulation: re-assessing the probability conditioning method for facies model calibration. *Computational Geosciences*, *23*(4), 683–703.

Mariethoz G., & Caers J. (2015), Multiple-point geostatistics: Stochastic modeling with training images, First edition.

Mariethoz, G., McCabe, M. F., & Renard, P. (2012). Spatiotemporal reconstruction of gaps in multivariate fields using the direct sampling approach. *Water Resources Research*, *48*, W10507. https://doi.org/10.1029/2012WR012115

Mariethoz, G., Renard, P., & Straubhaar, J. (2010). The direct sampling method to perform multiple-point geostatistical simulations. *Water Resources Research*, *46*, W11536. https://doi.org/10.1029/2008WR007621

Meerschman, E., Pirot, G., Mariethoz, G., Straubhaar, J., Van Meirvenne, M., & Renard, P. (2013). A practical guide to performing multiple-point statistical simulations with the Direct Sampling algorithm. *Computers and Geosciences*, *52*, 307–324. https://doi.org/10.1016/j.cageo.2012.09.019

Renard, P., & Allard, D. (2013). Connectivity metrics for subsurface flow and transport. *Advances in Water Resources*, *51*, 168–196. https://doi.org/10.1016/j.advwatres.2011.12.001

Straubhaar, J. (2017), User's Guide May 2017 DeeSse Software patented by the University of Neuchâtel, Tech. rep., University of Neuchâtel.

Straubhaar J., Renard P. & Chugunova T. (2020), Multiple-point statistics using multi-resolution images. *Stochastic Environmental Research and Risk Assessment*. https://doi.org/10.1007/s00477-020-01770-8

Strebelle, S. (2002). Conditional simulation of complex geological structures using multiple-point statistics. *Mathematical Geology*, *34*(1), 1–21. https://doi.org/10.1109/CEC.2011.5949612

Tarantola, A. (2005), Inverse problem theory and methods for model parameter estimation, Society for Industrial & Applied Mathematics, Philadelphia.

Zahner, T., Lochbühler, T., Mariethoz, G., & Linde, N. (2016). Image synthesis with graph cuts: A fast model proposal mechanism in probabilistic inversion. *Geophysical Journal International*, *204*(2), 1179–1190. https://doi.org/10.1093/gji/ggv517

Zhou, H., Gómez-Hernández, J. J., Hendricks Franssen, H. J., & Li, L. (2011). An approach to handling non-Gaussianity of parameters and state variables in ensemble Kalman filtering. *Advances in Water Resources*, *34*(7), 844–864. https://doi.org/10.1016/j.advwatres.2011.04.014

Zhou, H., Gómez-Hernández, J. J., & Li, L. (2012). A pattern-search-based inverse method. *Water Resources Research*, *48*, W03505. https://doi.org/10.1029/2011WR011195

Zhou, H., Gómez-Hernández, J. J., & Li, L. (2014). Inverse methods in hydrogeology: Evolution and recent trends. *Advances in Water Resources*, *63*, 22–37. https://doi.org/10.1016/j.advwatres.2013.10.014

Zovi, F., Camporese, M., Hendricks Franssen, H.-J., Huisman, J. A., & Salandin, P. (2017). Identification of high-permeability subsurface structures with multiple point geostatistics and normal score ensemble Kalman filter. *Journal of Hydrology*, *548*, 208–224. https://doi.org/10.1016/j.jhydrol.2017.02.056